### Title

Magnetic resonance spectroscopy of the brain: a review of physical principles and technical methods




### Journal

Reviews in the Neurosciences, 26(6)

### ISSN

0334-1763



### Authors

Buonocore, Michael H
Maddock, Richard J



### Publication Date

2015

### DOI

10.1515/revneuro-2015-0010

Peer reviewed

# Magnetic resonance spectroscopy of the brain: A review of physical principles and technical methods

Michael H. Buonocore[1,2] and Richard J. Maddock[2,3]

Department of Radiology[1], Imaging Research Center[2], and Department of Psychiatry and Behavioral Sciences[3]
University of California Davis Medical Center, Sacramento, CA 95817, USA

Reprint requests should be sent to:

Richard Maddock, M.D.
Department of Psychiatry, University of California Davis
2230 Stockton Blvd.
Sacramento, CA, 95817
Phone: (916) 734-3286
Fax: (916) 734-8750
rjmaddock@ucdavis.edu

Running title: Physical principles and methods of MRS

The published version of this paper can be found at:

**Reviews in the Neurosciences 2015; 26(6): 609–632**

**Abstract**

Magnetic resonance spectroscopy (MRS) provides unique information about the neurobiological substrates of brain function in health and disease. However, many of the physical principles underlying MRS are distinct from those underlying magnetic resonance imaging, and they may not be widely understood by neuroscientists new to this methodology. This review describes these physical principles and many of the technical methods in current use for MRS experiments. A better understanding these principles and methods may help investigators select pulse sequences and quantification methods best suited to the aims of their research program and avoid pitfalls that can hamper new investigators in this field.

Key words: biophysics; echo time; neurochemistry; NMR; proton; pulse sequences

Magnetic resonance spectroscopy (MRS) is a non-invasive method for measuring the brain content of selected metabolites, including N-acetylaspartate, creatine, choline, glutamate, myo-inositol, lactate, GABA, and others. Increasing numbers of cognitive, behavioral, and clinical neuroscientists are incorporating MRS measures into their experimental designs. However, many aspects of the physical principles underlying MRS differ from those on which magnetic resonance imaging is based. These principles may not yet be widely understood by neuroscientists new to MRS. This review is motivated by the view that it will support the scientific goals of such investigators to have a basic understanding of the physical principles underlying these measures and the methods used to obtain them. Thus, this review provides physical explanations of the processes that give rise to the phenomena that can be observed in MRS experiments. It is hoped that newcomers to spectroscopy will gain greater ability to understand and select the most appropriate pulse sequences and quantification strategies for their scientific questions when this basic understanding of the physical processes is achieved. Although the review is limited to discussion of the properties of spectra obtained using the point resolved spectroscopic sequence (PRESS) (Bottomley 1984; Bottomley 1987), the concepts and principles covered here are applicable to MRS methods in general. The PRESS sequence is currently the most widely used excitation and localization scheme for MRS studies, and it is described in detail in section 2.2.1. However, other sequences, including STEAM (Stimulated Echo Acquisition Mode), LASER (Localization by Adiabatic SElective Refocusing), and SPECIAL (SPin ECho full Intensity Acquired Localized), offer advantages for specific experimental situations and can provide valuable alternatives to PRESS (Frahm et al 1989b; Garwood and DelaBarre 2001; Mlynárik et al 2006).

A comprehensive review of the basic physics of magnetic resonance imaging is not provided here. It is assumed that the reader already has knowledge of such basic concepts as longitudinal and transverse magnetization, nutation of magnetization by radiofrequency pulses, and the process of precession of transverse magnetization by the application of the main magnetic field and fields due to magnetic field gradient pulses. Also assumed is an understanding of the process of spatial encoding using frequency and phase encoding for 2D or 3D imaging. For this and related background knowledge, the reader is referred to standard textbooks on the chemistry and physics of nuclear magnetic resonance (NMR) (Levitt 2008), to standard MRI texts covering the physics and engineering of MRI (Haacke et al. 1999; Edelman 2006), to standard texts on the application of NMR and imaging methodologies for in-vivo spectroscopy (De Graaf 2007), and to handbooks that provide physical constants for biologically important elements and NMR chemical shift and J-coupling values for typical molecular bonds (Dean 1992). Operators' manuals from major MR system manufacturers also provide concise information on the physics of MRS (Kohler 1993; General_Electric 1999; Siemens 2004; Siemens 2002). Finally, the textbook by Tofts on quantitative MR of the brain (Tofts and Waldman 2003) includes a concise yet thorough chapter covering key concepts, considerations and procedures, along with many valuable citations. Information from these cited sources has been used for the introductory parts of this review.

### 1.1 Characteristics of the Magnetic Resonance Spectroscopy Signal

Magnetic Resonance Spectroscopy (MRS) refers to the use of the magnetic resonance phenomenon to determine the relative concentrations of specific molecules in the sample under investigation. The key output of MRS is a magnetic resonance spectrum (MR spectrum), which

graphically displays the detected signals as a function of their temporal frequencies. In distinction, Magnetic Resonance Imaging (MRI) refers to the use of the magnetic resonance phenomenon to generate spatially resolved images based on the signals from the protons in bulk water and lipids within the sample under investigation.

The signal used to create MR spectra arises from the nuclei in the atoms of the individual molecules of the tissue sample. Although the application of MRS in clinical medicine is based primarily on detection of signal arising from the hydrogen nuclei (i.e. protons) present in the molecules of the human body, many other nuclei found in the body can also generate MR signals. A listing of the most important of these elements for clinical MRS is given in the Table. Every nucleus that can generate an MRS signal has a non-zero intrinsic magnetic moment, which can be manipulated by the application of external magnetic fields. The intrinsic magnetic moment is a consequence of the intrinsic spin of the nuclei, which arises from the quantum mechanical intrinsic spin of the individual protons and neutrons that comprise each nucleus.

### 1.1.1 Nuclei that Can Provide MR Signal from the Body

Generally, a nucleus will possess a non-zero magnetic moment and hence can generate an MR signal if the number of protons (given by atomic number Z) is odd, or if the number of neutrons (given by atomic mass number (N) minus the atomic number Z, or N-Z) is odd, or both numbers are odd (Gautreau and Savin 1978). Individually, a proton and a neutron each have an intrinsic spin of ½, and an intrinsic magnetic moment of 14.106 x 10^-27 Joules/Tesla and -9.662 x 10^-27 Joules/Tesla, respectively (see the Table for additional details). Within any nucleus, protons tend to "pair up" with their intrinsic spins in opposite directions. Consequently, the magnetic moments of these paired protons are in opposite directions, and they contribute zero magnetic

moment to the total magnetic moment of the nuclei. The same effect occurs with neutrons. Thus, nuclei with an even number of protons and an even number of neutrons will most likely possess a zero magnetic moment. This pairing of protons and neutrons is indicative of the lowest energy state of the nucleus with respect to intrinsic spin, which at body temperature is the state of virtually all nuclei.

The body is composed of many naturally occurring elements with nuclei that can generate an MR signal (so-called MR active elements), such as Hydrogen ($^{1}H_{1}$), Nitrogen ($^{14}N_{7}$), Oxygen isotope ($^{17}O_{8}$), Sodium ($^{23}Na_{11}$), Phosphorus ($^{31}P_{15}$), Potassium ($^{39}K_{19}$), Calcium ($^{41}Ca_{20}$), and the Carbon-13 isotope ($^{13}C_{6}$). This notation provides the atomic mass number as a superscript preceding the element initials, and the atomic number as a subscript. By far the most common occurring element is $^{1}H_{1}$. The main isotope of carbon is $^{12}C_{6}$, with 6 protons and 6 neutrons, and the principle isotope of oxygen is $^{16}O_{8}$, with 8 protons and 8 neutrons. Unfortunately, neither of these main isotopes has net magnetic moment or is MR active.

The main challenge in using MRS with molecules other than water is their low biological concentration. For MR imaging (not spectroscopy), the hydrogen atoms in bulk water within tissues serves as an immense resource of protons. The biological abundance of hydrogen from water within tissue is approximately 65 moles/liter. Although bulk water provides ample signal for imaging and allows for high spatial resolution (e.g. 1 microliter voxel size), detection of bulk water is not the motivation for MRS. Proton MRS experiments rely on the hydrogen atoms in the biologically important small molecules that are typically in millimolar (mM) concentrations, many orders of magnitude less than the concentration of hydrogen atoms in bulk water. Phosphate containing compounds occur in brain in concentrations 5-15 mM (adenosine phosphates, phosphocreatine, inorganic phosphates, etc.). However, $^{31}P$ nuclei

provide considerably less signal than do $^{1}H$ nuclei (Table). To obtain good quality $^{31}P$-MRS spectra, it is usually necessary to use large voxels and scan times of 12 to 20 minutes or more (De Graaf 2007). For a given nucleus, achievable voxel size reflects the concentration of the metabolite or ion. The higher the concentration, the smaller the voxel size required to obtain reasonable signal.

### 1.1.2 Generating the MRS Signal

In the presence of an external static magnetic field, an energy difference occurs between nuclei whose magnetic moments are aligned with, versus aligned against, the static magnetic field. The lower energy state is the one with the magnetic moment aligned with the static field. The presence of a static external magnetic field results in a slightly greater number of protons to be in the low energy state relative to the higher energy state, and thus generates a net magnetic moment, referred to as the magnetization. The magnetization is the net magnetic moment in each voxel that generates an MR signal, and exists for every voxel defined in the MRS experiment. In each voxel, the Thermal Equilibrium Magnetization is a stable configuration of magnetization, representing the maximum magnetization that results from the excess of nuclei that are aligned with the static magnetic field. For proton MRS on 1.5T systems, the thermal equilibrium magnetization is formed by just five more protons in the low energy state compared to the high-energy state, for every one million protons in the voxel. By convention, a proton in the low energy state, with its intrinsic magnetic moments aligned with the static magnetic field, is called a spin-up proton in reference to the proton's intrinsic spin that is also aligned with the magnetic field. Similarly, a proton in the high energy state, with its intrinsic magnetic moment aligned against the static magnetic field, is called a spin-down proton.

Generally, for magnetization to generate an MR signal, it must exist in the transverse plane. Generation of transverse magnetization is accomplished with radiofrequency (RF) pulses that provide energy for the magnetization (which forms automatically as the magnetization approaches thermal equilibrium) to be rotated away from the longitudinal axis, and into the transverse plane. When magnetization is in the transverse plane, it rotates at a characteristic frequency (the Larmor frequency) and creates a magnetic field that can be detected by a radiofrequency coil. This rotation is referred to as precession. The magnetization carries with it a dipole magnetic field that extends well outside the body, and so a precessing magnetization carries with it a rotating dipole magnetic field. At any location outside of the body the magnetic field created by the magnetization appears to be rapidly changing in time, because of the rotation. Faraday's Law of Electromagnetic Induction explains the generation of an oscillating electromotive force (emf) in the conducting material of an external RF coil from this rotating dipole magnetic field. In other words, given a circular loop of conductor placed outside of the body, the changing magnetic field created by the precessing magnetization creates an oscillating emf within the conductor. This emf drives an oscillating electric current in the RF coil.

In the presence of an applied magnetic field, the precessing transverse magnetization has a characteristic temporal frequency of precession, which is linearly proportional to the strength of the applied magnetic field. This temporal frequency of precession is called the Larmor frequency. Each nucleus possesses a fundamental constant, called the gyromagnetic ratio ($\gamma$), which is directly related to the nucleus' magnetic moment. In fact, any nucleus that has a non-zero magnetic moment will also have a non-zero gyromagnetic ratio. The Larmor frequency is calculated by multiplying the nucleus' gyromagnetic ratio with the strength of the magnetic field that the magnetization experiences. The Larmor frequency is the temporal frequency at which the

emf will be generated within the RF coil. The Table gives the gyromagnetic ratios for the common biological nuclei, and also gives the Larmor frequencies at 1.5T field strength (for the Larmor frequency at 3.0T, multiply the numbers in that column by 2).

In its simplest form, a radiofrequency coil is a loop of conducting wire that is tuned to have a specific low resistance to current flow at and around the Larmor frequency of the main magnetic field. The RF coil must be placed so that the dipole magnetic field generated by the precessing transverse magnetization creates magnetic field changes within the cross-sectional area defined by the loop of the RF coil. The requirements for placement of the RF coil around the brain are the same as they are in imaging. Specifically, the axis of the RF coil (defined as the direction perpendicular to the plane containing the loop of conducting wire of the coil) must be perpendicular to the main magnetic field. This orientation ensures that the changing magnetic field from the precessing magnetization vectors induces an electromotive force in the conducting wire, in accordance with Faraday's Law of Electromagnetic Induction. The current generated by the emf is directly proportional to the magnitude of the magnetization that is precessing. This proportionality is what enables MRS to provide spectra that reflect the concentration of the signal source.

### 1.1.3 Basic Characteristics of an MRS Spectrum

An MRS spectrum is derived from the signal emanating from the magnetization vectors precessing in the transverse plane. The axes of the one-dimensional spectrum are temporal (i.e., precession, or Larmor) frequency on the horizontal axis, and amplitude on the vertical axis. Frequency can be represented as cycles/second (Hz). For an MRS spectrum, a zero frequency is identified, defined as the Larmor frequency of a reference molecule at the field strength being

used. That molecule is tetramethylsilane (TMS) for proton MRS spectra displayed on clinical MRI systems. The Larmor frequencies of the metabolite protons can also be represented in parts per million (ppm) relative to the Larmor frequency of the reference molecule in the magnetic field strength being used. For example, for a 1.5 Tesla system used for proton spectroscopy, the Larmor frequency of TMS is 63.86 MHz (set to 0 ppm), and on the spectrum, 1 ppm on the horizontal axis represents 63.86 Hz of chemical shift. On a 3 Tesla MRI system, the Larmor Frequency of TMS is 127.7 MHz (set to 0 ppm), and 1 ppm represents 127.7 Hz of chemical shift. Figure 1 illustrates typical brain 1H-MRS spectra obtained at short (TE 30 ms) and long (TE 144 ms and 288 ms) echo times. The biochemical nature and neurobiological significance of the molecules observed in such spectra have been reviewed elsewhere (Govindaraju et al. 2000; Maddock and Buonocore 2012; Rae 2014).

In all MR spectra, the signal from any specific metabolite protons does not occur at a single Larmor frequency, but is spread out over a narrow range of frequencies due to the inherent T2 relaxation of the transverse magnetization, and due to the magnetic field (B0) inhomogeneity within the voxel. T2 relaxation occurs during the long (e.g. 819.2 ms) acquisition period and causes a distinct spreading of the peak in the temporal frequency domain, which is characterized by the linewidth (full width at half maximum) of the peak. Also, the range of magnetic field values within the voxel results in a range of Larmor frequencies, and this range of Larmor frequencies is manifested in a spreading of the spectral peak. Figure 2 shows four spectra, one with very narrow linewidth and three others with increasingly wide linewidths. In these spectra, increases in linewidths are due to increases in B0 inhomogeneity. In each spectrum, the linewidth contribution from the T2 of the nucleus, and the linewidth contribution from the B0 inhomogeneity are approximately additive.

## 1.2 Types of Interactions that Can Be Detected with MRS

### 1.2.1 Chemical Shift

The electron orbitals in a molecule generate local magnetic fields, which change the magnetic field that is experienced by the nuclei in the molecule. As a result, each nucleus exists in a unique magnetic field microenvironment created by the applied external magnetic fields and by the electrons surrounding the nucleus. Thus each nucleus in a molecule has a Larmor frequency that is slightly different from the Larmor frequencies of other nuclei in different locations in the same molecule or in other molecular species. The chemical shift of the nuclei is defined as the difference between the Larmor frequency of the nuclei and the reference molecule, TMS (Dean, 1992). All nuclei that are equivalently positioned within a molecule will have the same chemical shift. However, the chemical shift is determined not only by the molecular structure but also the dynamical properties of the molecules and its bonds. For example, although the three protons in a methyl group occupy different physical locations within a molecule, these protons will typically have the same chemical shift. The result is explained by the dynamics of the molecular bonds. The methyl group is rapidly rotating around the C-C bond connecting the methyl group to the rest of the molecule, and also the molecule itself is freely rotating. Consequently, the protons in the methyl group have equivalent average locations, and experience equivalent magnetic shielding over the time interval of signal acquisition needed for Larmor frequency identification. As a result, the same chemical shift is measured in each proton of the methyl group. A typical MRS spectrum reveals the chemical shifts of all of the observable nuclei in the molecules of the sample.

### 1.2.2 J-Coupling

In some molecules, the electron orbitals form molecular orbitals that generate coupling between adjacent nuclei within the molecule, the most common example of which is referred to as "J-coupling". Coupling introduces a distinct set of changes in the Larmor frequencies that are identifiable on the spectrum. The J-coupling effect is always mutual; if nucleus A affects the precession frequency of nucleus X through J-coupling, then nucleus X affects nucleus A. J-coupling in all of its different forms is complex and varied within a molecule, and it can produce complicated patterns of spectral peaks. Complete listings of J-coupling values and chemical shift values for spectral peaks in important biological molecules are available (Govindaraju et al. 2000; Dean 1992; De Graaf 2007). In the next section, we will illustrate the essential features of J-coupling using the example of the lactate molecule (CH3COHCOOH), which has three equivalent protons in a methyl group (CH3) J-coupled to a single hydrogen proton in a methine group (CH). The molecular structure and its relevance to determining the chemical shift and J-coupling effects are shown in Figure 3. The J-coupling effects most commonly observed in clinical MRS are based on coupling between protons on adjacent carbon atoms, i.e. between protons acting through a single C-C bond. Although lactate is used exemplify J-coupling effects here, other important molecules in the brain exhibit J-coupling effects, including glutamate, glutamine, myo-inositol, GABA and glutathione. Some of these molecules (e.g. GABA and glutathione) are most reliably detected on clinical scanners when using pulse sequences that specifically take advantage of their J-coupling effects (Mescher et al. 1998; Terpstra et al. 2003).

### 1.2.3 Singlet, Doublet, and Other Spectral Peaks in MR Spectra

Singlet, doublet, triplet and higher order multiplet spectral peaks are present in brain MR spectra. The simplest peak structure, the singlet, arises from nuclei that are not coupled to other nuclei in the same molecule. The peak arising from NAA at 2.01 ppm is a singlet (Figure 1). If a nucleus is affected by J-coupling, the peak will be "split" into two or more distinct peaks. This splitting of the peaks is a result of different Larmor frequencies of this nucleus existing in the many molecules that contribute to the total signal reaching the coil. The simplest case of J-coupling is when, within each molecule, one nucleus (denoted A) is J-coupled to one other nucleus (denoted X). Figure 4 illustrates this coupling of nuclei A and X, showing that the A peak is split into two peaks (a doublet). If nuclei A and X were not J-coupled, nucleus A would generate a singlet at the Larmor Frequency denoted by $\delta_A$ in the figure. However, since they are J-coupled, 50% of the molecules in the sample have nucleus X with its spin oriented spin-down (as shown on the left of Figure 4). In these molecules, nucleus A contributes signal at the Larmor frequency denoted by $\delta_A + J/2$. The other 50% of the molecules have nucleus X oriented spin-up (as shown on the right of Figure 4). In these molecules, nucleus A contributes signal at the Larmor frequency denoted by $\delta_A - J/2$. Thus, nucleus A gives rise to two spectral peaks separated by J Hz in the frequency domain.

In lactate, the methine proton splits the peak from the protons of $CH_3$ into a doublet, by the mechanism explained above. Figure 5a illustrates the spin orientations of the methine group proton, and how it affects the signal from the three methyl group protons. If the J-coupling were not present, the three methyl protons would generate a large singlet at 1.32 ppm on the spectrum. However, the J-coupling of each of these methyl group protons to the methine (C-H) proton converts the singlet to a doublet. The J value separating the doublet peaks is 6.93 Hz for lactate, and each peak of the doublet has equal peak areas. For lactate molecules that possess a spin-

down methine proton, the magnetic field at each of the methyl protons is increased, which increases the Larmor frequency of the methyl protons. Hence, the location of the peak in the spectra is shifted toward higher frequency by J/2 Hz. Similarly, for lactate molecules that possess a spin-up methine proton, the magnetic field at each of the methyl protons subtracts from the main magnetic field, and decreases the Larmor frequency of the methyl protons by J/2 Hz. Hence, the methyl protons appear in the spectra as two peaks. The three protons of $CH_3$ split the peak from the single proton of the methine group into a quartet. This is because 50% of the coupled methyl protons are spin-up, and 50% are spin-down, and within any molecule the instances of spin-up and spin-down are randomly determined. Figure 5b illustrates all the possible combinations of spin orientations of the methyl group protons that are coupled, and how they affect the signal from the methine proton. The methine proton peak is split into 4 distinct peaks, with intensities in the ratio 1:3:3:1. The amount of shift explains the location of each peak of the quartet on the spectra, and the number of combinations of spin-up and spin-down states explains the size of each peak of the quartet.

### 1.2.4 Relaxation Times of Spectral Peaks

In imaging we are familiar with observed longitudinal (T1) relaxation times and transverse (T2) relaxation times of the water and of the fat that is imaged at each voxel of the image. In spectroscopy, each set of nuclei giving rise to a specific resonance represented in the spectrum will have a unique T1 and T2. Importantly, T1 and T2 will affect the strength of the observed signal, and this will confound direct use of the signal strength for estimating the absolute metabolite concentration. As with water protons, these T1 and T2 values are dependent on the local molecular environment. The tissue dependent T1 and T2 associated with the most

prominent spectral peaks in 1H-MRS spectra from human brain have been studied by several investigators, e.g. (Frahm et al. 1989a; Kreis et al. 1993; Kreis 1997; Mlynárik et al. 2001; Träber et al. 2004), and the compiled data has been proposed for use in approaches to quantitative MRS (see Section 5.1.2 below). The main mechanisms contributing to the observed T1 and T2 of a specific nucleus are the same as the mechanism of T1 and T2 in bulk water, although additional intramolecular mechanisms also contribute. The T1 of the signal is smallest (i.e. "shortest") if the molecule is tumbling at an instantaneous rate of rotation that is the same as the Larmor Frequency for that nucleus. Such tumbling causes increased relaxation (i.e. shorter T1) because local magnetic fields influencing each nucleus are then rotating at the Larmor frequency and able to generate transitions between the spin-up and spin-down states of the nuclei. Since these transitions are occurring randomly in time and influence the metabolite nuclei uniquely, the alignment of the nuclei's magnetic moments within the voxel is gradually lost and the magnetization decays. Thus, as with T1, the T2 relaxation time is reduced if the characteristic frequency of tumbling of the molecule matches the Larmor frequency. However, T2 is shortened further by the "static dephasing" term, which is the contribution to spin dephasing from molecules that are rotating extremely slowly (e.g. characteristic time about 1–10 ms). Due to this static dephasing term, a particular tissue's T2 relaxation time is always shorter than its T1 relaxation time.

## 2.1 Pulse Sequences for Single Voxel Spectroscopy and Chemical Shift Imaging

### 2.1.1 Single Voxel MRS

Single voxel spectroscopy (SVS) refers to the process of using the magnetic field gradients in a pulse sequence to define a 3D cubical region (a voxel) from which the transverse magnetization

of the metabolite nuclei generate signal. The localization process of an SVS pulse sequence serves to limit the brain volume from which signal arises during data acquisition. Additional RF and field gradient pulses, called saturation pulses, are typically also applied in the pulse sequence to ensure that magnetization outside of this defined voxel does not contribute signal. The point resolved spectroscopic sequence (PRESS) (Bottomley 1984; Bottomley 1987) is commonly used by researchers for localization and is described here.

Because in-vivo metabolites are in millimolar concentrations, voxel sizes must be sufficiently large to obtain enough signal to generate a high quality spectra. For example, NAA (which has three equivalent protons contributing to its peak at 2.01 ppm), creatine (which has groups of 2 and 3 equivalent protons contributing to singlet peaks at 3.92 ppm and 3.03 ppm respectively), and choline (which has 9 equivalent protons from 3 methyl groups contributing to its singlet peak at 3.21 ppm) provide proton concentrations (number of contributing protons per molecule times the concentration of the molecule) in an approximate range of 10 to 30 mM. Measurement of these molecules typically uses voxel sizes of 8 cc (e.g., 2 cm x 2 cm x 2 cm) or greater. Lactate, which has three equivalent protons contributing to its doublet, provides lower proton concentrations of approximately 1.0 – 3.0 mM in normal subjects. Lactate measurement typically uses voxel sizes of about 15 to 30 cc or greater. GABA gives rise to three resonances, each having two equivalent protons contributing to its multiplet. One of these (at ~3.0 ppm) is quantified by the most commonly used GABA measurement technique on clinical scanners (MEGA-PRESS) and has a proton concentration of approximately 2.0 – 4.0 mM (Mescher et al. 1998). GABA measurement typically uses voxel sizes of about 10 to 25 cc or greater. The need for large voxel sizes, and the resulting poor spatial resolution of the information extracted from the spectra, is one of the main limitations of MR spectroscopy.

In preparation for a single voxel MRS scan, the MRI system shims the magnetic field by adjusting the electric currents in the shim coils. Shim coils are an integral part of the MR system, typically constructed within the same annular structure as the gradient coils used for imaging, and produce magnetic fields with approximate polynomial dependence on the spatial coordinates x, y and z within the imaging volume. Through an iterative shim procedure available on all commercial 3T systems, the electrical current values for linear and quadratic shimming are adjusted to provide the most uniform magnetic field within the prescribed voxel.

The PRESS sequence consists of a series of RF and gradient pulses that define the voxel, followed by a time interval for data acquisition. As illustrated in Figure 6, voxel definition is accomplished by sequentially applying slice selective gradients in each of the three orthogonal directions. First, a 90 degree RF pulse is applied with the physical x gradient simultaneously turned on. This combination produces a slab of excitation parallel with the y-z plane. Later (typically within ten ms), a 180 degree RF pulse is applied with the physical y gradient simultaneously turned on. This combination creates a slab of transverse magnetization parallel with the x-z plane. Within the columnar volume defined by the intersection of these two slabs, this pulse acts as a 180 degree pulse that refocuses the transverse magnetization. Finally, a 180 degree RF pulse is applied with the physical z gradient simultaneously turned on. This combination selects a slab of excited magnetization parallel with the x-y plan. Within the cubical volume defined by the intersection of all three slabs, this pulse acts as a 180 degree pulse that refocuses the transverse magnetization. Thus, the sequence of these three RF pulse-gradient combinations results in a small cubical volume of magnetization. Only in this defined 3D voxel will the transverse magnetization generated by the initial 90 degree pulse refocus to produce a significant signal. All magnetization not located within the cubical volume will either be

longitudinal (having not experienced any of the RF pulses), or will be in the transverse plane but not refocused, and will not produce any appreciable signal.

Within each TR interval, the exact time of refocusing of the transverse magnetization in the defined voxel, called the echo time (TE), is determined by the timing intervals between the RF pulses of the sequence. The TE is defined as the time interval between the initial 90 degree excitation pulse, and the time when refocusing of the transverse magnetization occurs within the three-dimensional voxel defined by the PRESS sequence. The dephasing and subsequent rephasing of magnetization, as the voxel is being defined, is illustrated in Figure 7. An echo time of TE is obtained by separating the $1^{st}$ and $2^{nd}$ 180 degree pulses by an interval TE/2. The time interval $\Delta t$, defining the time between the 90 degree pulse and first 180 degree pulse, is typically chosen to be as short as possible, but sufficiently long to allow the gradient pulses to be played out. At TE, the magnetization within the voxel is fully rephased and yields maximal signal. The term "echo" refers to the long time interval around the TE when signal from the magnetization can be readily detected. The time of maximal signal at TE is often referred to as the "echo center". Unlike imaging, where the pulse sequence is set up so that the echo center occurs in the middle of the data acquisition window, in PRESS the pulse sequence timing requires that the echo center occur near the beginning of the data acquisition. In single voxel MR spectroscopy, data acquisition begins within 10-20 ms before TE and typically extends for 800-1000 ms after TE. The exact duration of the data acquisition depends on several user defined settings as well as settings defined by the MR system manufacturer. The number of data points collected in each acquisition, and the time interval between each data point, is determined by the desired frequency resolution of the spectrum (spectral resolution) and frequency range of the spectrum. The spectrum must have a certain minimum possible spectral resolution, measured in Hz, for

detection and separation of the metabolite peaks. The spectrum must also separate received signal over a certain range of temporal frequencies, called the spectral range, so that all of the spectral peaks of interest will be found within the range, and also so that any signals from outside of that range do not overlap the peaks of interest. The spectral resolution in Hz is determined as the reciprocal of the total time duration of the data acquisition in seconds, and the spectral range is determined as the reciprocal of the sampling interval, or the temporal spacing in seconds between successive data points collected during the data acquisition. For example, on a 1.5 Tesla system running a basic PRESS sequence, the total data acquisition time can be set at 819.2 ms, thus producing spectra with a spectral resolution of 1.2 Hz, and the sampling interval can be set at 0.4 ms, corresponding to a spectral range of 2500 Hz. By dividing the total data acquisition time by the sampling interval, we compute that 2048 data points are acquired in a MRS data acquisition using these parameters. On a 3.0 Tesla system, the total acquisition time may be set at 1024 ms, corresponding to a spectral resolution of 0.98 Hz, and the sampling interval may be set at 0.5 ms, corresponding to a spectral range of 2000 Hz, from which we compute that 2048 points are collected using these parameters. Clinical MR systems provide default values for data collection that for the majority of clinical applications do not need to be changed to get reliable, high quality spectra.

### 2.1.2 2D and 3D Chemical Shift Imaging

While single voxel MRS provides a robust method for obtaining a large signal from a specific brain region, 2D and 3D chemical shift imaging (CSI) are designed to cover larger brain regions and provide spatially resolved spectra throughout the selected plane or volume. CSI, whether 2D or 3D, can be used to investigate the entire brain, however it is typically used to analyze specific

brain regions at higher resolution than can be provided with SVS. CSI differs from SVS in that the "excitation voxel" created by the RF pulses is then subdivided into "resolution voxels" by the phase encoding process. In CSI it is important to distinguish between the excitation voxel created by the sequence of three RF pulses (similar to PRESS), and the multiple "resolution voxels" which are created as a grid in the spatial encoding process.

The name "chemical shift imaging" derives from the fact that the pulse sequence acquires a spectrum at each voxel within a two or three dimensional grid. Instead of reconstructing a single intensity value for each voxel as in MRI, in CSI an entire MR spectrum is reconstructed at each voxel. Since MR spectra are displays of the signal from nuclei with different chemical shifts, the term chemical shift imaging is appropriate. However, J-coupling effects between nuclei are also manifested on these MR spectra.

Data acquisition in CSI is exactly as described for single voxel spectroscopy. As in SVS, the signals can be resolved by measuring over a sufficient total acquisition time and sampling interval. The requirement to measure these signals while the echo is occurring precludes the use of frequency encoding as a means of creating spatial resolution. Thus, phase encoding is used for all spatial directions to obtain spatially resolved spectra. For example, if 2D CSI is performed with 8 phase encoding steps in each of two directions, a spectrum will be reconstructed in each voxel of an 8 x 8 grid of voxels, giving a total of 64 unique spectra from 64 unique spatial regions. If 3D CSI is performed with 8 phase encoding steps in each of three directions, a spectrum will be reconstructed in each voxel of an 8 x 8 x 8 grid of voxels, giving a total of 512 unique spectra from 512 unique spatial regions. In 2D and 3D CSI, the slice or slab thickness is determined by the slice or slab selection as done in standard imaging. Figure 8 displays the basic 2D CSI sequence, which can be understood as a PRESS sequence combined with phase encoding

gradients in two spatial directions, which are varied in each TR period to obtain the necessary range of spatial encoding. Figure 9 displays the array of spatially resolved MR spectra (called a "spectral map") obtained from a 16 x 16 2D CSI acquisition. Each spectrum has the same frequency resolution and range that is typically obtained in single voxel spectroscopy.

With a relatively small excitation voxel, shimming within the excitation voxel is consistently more successful (i.e., yields a narrower linewidth indicating reduced magnetic field inhomogeneity). Typically, the grid of spatial resolution voxels is extended outside of the excitation voxel, so that spurious signals from outside of the excitation voxel are not phase wrapped into the excitation voxel. However, using a large number of phase encode steps is uncommon for two reasons. First, it requires very long scan times, e.g. an 8 x 8 x 8 acquisition with TR 1.5 seconds requires 768 seconds. Second, for a fixed excitation voxel, the signal-to-noise ratio (SNR) of the spectra in each resolution voxel decreases as the number of phase encode steps increases, due to the smaller size of the resolution voxel. Unlike 2D CSI, which typically uses a slice thickness of 15-20 mm, 3D CSI typically uses a much greater slice thickness (e.g. 80-120 mm). This is because subsequent phase encoding will create multiple smaller resolution voxels along this dimension (e.g., 10-15 mm). A large number of resolution voxels will necessitate a long scan time for a CSI study. This is primarily because only one phase encode step can be set up in each TR interval. Thus, acquiring an N x M x P grid of spatially resolved spectra will take TR*N*M*P seconds.

The primary advantage of CSI over SVS is spatial resolution. The SNR of a CSI acquisition is equivalent to the SNR of a SVS acquisition for any given duration of acquisition. However, the CSI acquisition provides information about metabolite concentrations across a range of spatial locations. The primary disadvantage of CSI is that the quality of the shim is

typically worse than that of SVS. In CSI, shim currents are chosen to eliminate magnetic field inhomogeneities extending over the entire excitation volume. However, more subtle field inhomogeneities within each voxel of the grid are not eliminated. In general, inhomogeneities can be reduced to a greater extent in the volume of an SVS voxel than in the resolution voxels of a CSI acquisition. Thus, linewidths tend to be greater and more variable in the resolution voxels of CSI than in an SVS voxel.

### 2.1.3 Proton Echo Planar Spectroscopic Imaging

The Proton Echo Planar Spectroscopic Imaging (PEPSI) pulse sequence (Posse et al. 1995; Posse et al. 1997), cleverly interleaves the acquisition of the echo for spectral estimation with spatial encoding. This technique replaces one direction of phase encoding normally done in 2D or 3D CSI, with frequency encoding. For the development of PEPSI, Posse recognized that frequency encoding could be accomplished during the time intervals between the acquisitions of successive data points needed for generating the spectra. The opportunity to do frequency encoding comes from the fact that the sampling interval between data points needed for generating the spectra is very long, e.g. 400 ms for a frequency range of 2500 Hz and 833.3 ms for a range of 1200 Hz. The PEPSI sequence was made possible by the development of MRI systems with very fast gradients that were able to perform frequency encoding in that same (400-800 ms) time frame. For example, using a gradient of 30 mT/m over a 22 cm FOV, 64 data points for frequency encoding can be acquired in approximately 340 ms, indicating that the frequency encoding can easily be performed during the time between sampling points for spectroscopy.

That frequency encoding and spectral encoding could be interleaved was the significant insight that led to the development of the PEPSI pulse sequence. With removal of one dimension

of phase encoding, fast, spatial resolved spectroscopic imaging (Fast CSI) becomes a reality. Furthermore, fast 3D CSI becomes practical with PEPSI. Unfortunately, the interleaving scheme has subtle negative effects on the quality of the spectra within each voxel, so the sequence is not yet in widespread use. Nevertheless, PEPSI continues to be improved, with variants developed for advanced spectroscopic techniques (e.g. 2D correlated spectroscopic imaging) (Lipnick et al. 2010). Similarly, fast CSI methods based on the use of spiral gradients also significantly reduce scanning times and represent a promising approach for neuroscience and clinical studies (Adalsteinsson et al. 1998; Bogner et al. 2013).

### 3.1 Features of the MRS Pulse Sequence

#### 3.1.1 Dependence of spectrum appearance on echo time

Selecting the echo time (TE) is a critical factor in determining the appearance of the acquired spectra. T2 relaxation decreases the transverse magnetization throughout the time of the three RF pulses up to the echo time TE and also throughout the duration of data acquisition. Lengthening the echo time simplifies both the baseline and the pattern of peaks in the spectra. T2 relaxation time can vary considerably across the metabolites observable in human brain (Taber et al. 2004; Ganji et at. 2012). Signal from methyl and methylene protons in lipids generates broad peaks with relatively short T2s at 0.9 and 1.3 ppm. These peaks are often prominent in spectra obtained with short TE, but typically do not appear in spectra obtained with TE over 200 ms. Peaks from protons in myo-inositol are prominent when the spectra are obtained with TE 35 ms, but less visible when the spectra are obtained with TE over 100 ms. Peaks from metabolite protons with longer T2s are clearly visible at both short and long TEs (Figure 1).

TEs with particular values are often selected to reveal peaks that are optimally identified at those echo times. For example, TE 144 ms and 288 ms are often used to identify the signal from lactate. Due to J-coupling, as described in section 1.2.2 above, the lactate methyl protons give rise to a doublet centered at 1.32 ppm. During a 144 ms TE, J-coupling causes each group of methyl protons to accumulate 180 degrees of phase angle, thus causing them to appear negative on the spectra. This "inverted doublet" of the lactate molecule is a distinctive feature of the in-vivo proton spectra at 144 ms TE. At 288 ms TE, the phase angle accumulation is twice that of the accumulation at 144 ms TE. Consequently, the phase angle accumulation is positive or negative 360 degrees, and both peaks appear upright on the spectra. The effect of different TEs on the detection of metabolites with more complex J-evolution dynamics, such as glutamate, glutamine and myo-inositol, is an active area of investigation (e.g., Thompson and Allen 2001; Schubert et al. 2004; Hancu and Port 2011).

### 3.1.2 Water suppression

The concentration of bulk water is on the order of 10,000 times greater than the concentrations of metabolites in the brain (i.e. 70 M versus 1-10 mM). If the signal from water is not reduced, it interferes with measurement of the much smaller concentrations of other metabolites. In an MRS pulse sequence, Water Suppression is typically accomplished with Chemical Shift Selective Suppression (CHESS) (Haase et al. 1985), which refers to a specific sequence of three RF pulses alternating with gradient pulses designed (and tuned with each patient) to greatly reduce the signal from the protons of the bulk water, while having little or no effect on magnetization of the metabolites. The RF pulses are centered on the water signal at 4.7 ppm, and with the gradient pulses, they have a limited frequency range of effectiveness so that metabolite signals are not

affected. The CHESS module can be included with any MRS pulse sequence to improve detection of biologically important metabolites. Figure 10 displays the typical CHESS module preceding a PRESS data acquisition. The effective spectral width of this CHESS module (i.e. the frequency range over which the module provides signal suppression) is typically set at 75 Hz, equivalent to about 1.2 ppm at 1.5T. Consequently, the effect of the CHESS module, which is centered on the water peak (at 4.7 ppm), does not affect any peaks that are less than 4.1 ppm and greater than 5.3 ppm. Hence, the data acquisition sequence that follows the water suppression pulses yields signal from the metabolites, while the magnetic moments of protons in water give no signal. For some clinical or experimental conditions, alternatives to the CHESS sequence may be more suitable for suppression of the water signal. Alternative water suppression sequences include VAPOR (VAriable Pulse power and Optimized Relaxation delays) (Tkak et al. 1999) and WET (Water suppression Enhanced through T1 effects) (Ogg et al. 1994). In some spectral-edited sequences, the editing pulses (described in Section 4.1.1 below) can provide sufficient water suppression, because part of the entire spectral band of the spectral-editing pulse can be positioned over the water peak (Mescher et al. 1998).

### 3.1.3 Spatial Saturation Pulses to Reduce Signal from Outside the Voxel

Although the PRESS sequence is widely used to define voxels, signal from outside the voxel is not completely eliminated by its method of voxel definition. Signals from outside the voxel, including lipid signals from outside of the brain, can create spurious contributions to the spectra peaks and add to the baseline, thus making accurate signal quantification more difficult. Spatial saturation pulses are routinely used for single voxel spectroscopy (SVS) and for 2D and 3D chemical shift imaging (CSI) to reduce spurious signal originating from outside the voxel.

Spatial saturation pulses consist of an RF pulse applied simultaneously with a gradient pulse, such that a relatively thick slab of tissue outside of the desired voxel is selected. Immediately after the RF pulse has ended and transverse magnetization has been created, the gradient field is increased in magnitude and applied for several more milliseconds in order to dephase the transverse magnetization and reduce the signal from this magnetization to zero. Each saturation pulse targets a wide slab of tissue (e.g. 4 to 8 cm) outside of the desired voxel. It is not unusual for the sequence to have six regions of saturation (saturation bands) around the voxel, adjacent to all 6 sides of the voxel. In the pulse sequence, saturation pulses are always applied just prior to the PRESS acquisition, and after Water Suppression pulses.

Because saturation pulses are very effective in reducing signal originating outside of the desired voxel, most MR systems include a graphical user interface for selecting and positioning the saturation bands. Generally, as the width of the saturation band increases, so does the transition region of the band where the flip angle of the saturation pulse is between 0 and 90 degrees. Depending on the type of RF pulse used, the recommended transition region is 10-50% of the saturation band width. To ensure that the effective size of the voxel is not reduced by the saturation pulses, the edge of the saturation band should be no closer to the voxel edge than 10-50% of the saturation band width, unless the system offers specialized saturation pulses. Because RF pulse technology is continuing to improve, it is advisable to check the documentation of your MRI system to determine the optimal placement of the saturation bands.

### 3.1.4 Averaging and Phase Cycling to Improve Signal to Noise Ratio

Averaging is a process of repeating the sequence of RF and gradient pulses and the signal acquisition a specified number of times, in order to add the signals. Adding the signals increases

the SNR in proportion to the square root of N, (Sqrt(N)), where N is the number of repetitions that are averaged. This Sqrt(N) dependence is the result of the fact that the signal from the magnetization detected in the RF coil is the same and hence adds linearly with each repetition, while the noise detected in the RF coil is random and thus does not fully add with each repetition. While the signal increases linearly in proportion to N, the noise increases only in proposition to Sqrt (N). Hence the SNR increases in proportion to Sqrt(N). A substantial number of repetitions, typically 64, 96, 128, 192, 256 or more, is necessary to obtain a high quality averaged spectrum. With TR 1500 ms, the scan times are in the range of 96 seconds to 384 seconds for the numbers of repetitions listed above. In the case of CSI, averaging is accomplished in each voxel of the grid during the process of phase encoding. For example, if an 8 x 8 grid is acquired in 2D CSI, each voxel of the grid acquires an SNR consistent with 64 repetitions, since during each TR, signal is acquired from every voxel in the grid.

Phase cycling is accomplished by repeating a pulse sequence and signal acquisition with all acquisition parameters the same except for the phase angle of the RF pulse, which is set to a specified angle for each repetition. Most spectroscopy sequences use the largest number of phase cycling steps that is compatible with the user-specified number of repetitions, applying up to 16 different phase angles in the phase cycle. One complete cycle of data acquisitions using the phase cycling method is often referred to as a "frame" of data. Phase cycling suppresses undesirable aspects of the signal, while providing the full SNR advantage of signal averaging. The simplest phase cycling scheme consists of two TR periods with the phase of the RF excitation pulses used in the second acquisition set at 180 degrees relative to the phase of that used in the first acquisition, causing a relative negative sign to exist between the data of the two acquisitions. In this simple scheme, the "frame" of data consists of data acquisitions from two

successive acquisitions. The data from the second excitation is subtracted from the data from the first acquisition, to produce a single line of data with twice the signal level, and only Sqrt(2) increase in the noise. In this scheme, the subtraction adds the signals from the first and second acquisitions, while the noise and certain electronic errors that are independent of the phase of the RF pulses are partially or fully cancelled by the subtraction.

### 3.1.5 Other Factors that Can Influence Spectral Quality

The slice-selective gradients for defining the spectroscopy voxel (described in section 2.1.1) can be generated in one of six possible orders. Under some circumstances, the gradient order can significantly influence the quality of the spectral signal. Ernst and Chang have shown that the optimal gradient order depends on the voxel location within the brain and that a suboptimal gradient order can increase contamination from signals originating outside the voxel (Ernst and Chang 1996 ). This can be particularly problematic at short echo times or when the resonances of interest are close to the lipid resonances (Maddock et al 2006; Maddock and Buonocore 2008). Gradient-induced drifting of the main magnetic field can also be problematic for MRS acquisitions. This can occur when imaging sequences that require high gradient duty cycles, such as fMRI or DTI, are acquired immediately prior to MRS acquisitions (Lange et al. 2011). This is particularly problematic when an MRS editing sequence is used, as it can reduce editing efficiency and increase subtraction errors (Harris et al. 2014). Head motion can also degrade the quality of spectral data (Bhattacharyya et al. 2007; Keating et al. 2010). Most investigators exclude clearly contaminated spectra based on visual inspection of the data. However, unlike with fMRI, there is not yet a generally accepted method for quantifying or correcting the effects of motion on MRS data.

### 4.1 Specialized Sequences for Isolating Overlapping Spectral Peaks

Other than chemical shift, the most prevalent interaction that is revealed in MR spectra is the J-coupling between hydrogen nuclei separated by single C-C bonds. Many investigators have described the effects of J-coupling on MR spectra obtained using the standard PRESS sequence (Ernst and Hennig 1991; Allen and Thompson 1999; Thompson and Allen 1999). These investigations supported the development and application of pulse sequences and analysis techniques that can exploit J-coupling to isolate the peaks of the J-coupled nuclei, and also to eliminate causes of signal cancellation (specifically volume misregistration). These sequences and techniques have improved our ability to measure signals from J-coupled nuclei.

#### 4.1.1 Spectral Editing: Isolating Spectral Peaks Based on J-Coupling

Isolating nuclei that are J-coupled (i.e. spectral editing) requires use of a pulse sequence that selectively excites the "coupled nuclei". The term "coupled nuclei" refers to the nuclei that are J-coupled to the nuclei providing the signal for the observed peak. The term "main nuclei" will be used to refer to those nuclei providing the signal for the observed peak. Two commonly used techniques that have been incorporated into the basic PRESS sequence to accomplish this selective excitation are called "MEGA" (Mescher et al. 1996; Mescher et al. 1998) and Band Selective Inversion with Gradient Dephasing (BASING) (Star-Lack et al. 1997; Star-Lack et al. 1998). Figure 11 illustrates BASING pulses within the PRESS sequence. These two techniques work on the same physical principles, and differ only in the details of the frequency selective RF pulses that are used. Selective excitation is achieved in MEGA and BASING using RF pulses that have a narrow frequency band matched to the Larmor frequency of the coupled nuclei.

When the coupled nuclei are selectively nutated with a 180-degree frequency-selective RF pulse, the precession direction of the J-coupling effect on the main nuclei is reversed (Hetherington et al. 1985). Consequently, if the J-coupling caused an increase in the Larmor frequency of a particular main nucleus before the selective RF pulse, then after the RF pulse the J-coupling will cause a decrease in the Larmor frequency of that nucleus. Applying the selective RF pulse enables precise control over the net effect that J-coupling has on the main nuclei. When the selective pulse is applied, the effect of J-coupling progresses during the entire duration of the voxel selection and data acquisition. When the frequency selective pulse is applied at some intermediate point of the timing of 90-180-180 PRESS sequence for voxel selection, then the J-coupling will have had a reduced final effect on the phase of the magnetization at the echo center. During the time prior to the selective pulse, J-coupling causes either a positive or a negative change in the Larmor frequency of the main nuclei, while during the time after the pulse J-coupling causes the opposite change. A zero net J-coupling effect is achieved when the time intervals of positive and negative change in Larmor frequency are equal to the entire duration of the PRESS volume selection prior to formation of the echo center. To achieve cancellation of the J-coupling effect in the PRESS sequence, two spectral-editing pulses must be applied, separated by TE/2 seconds. Figure 12 illustrates the specific timing of the spectral-editing pulses that yields cancellation of the J-coupling effect during PRESS voxel selection. With these pulses, positive and negative precession directions of the J-coupling effect each occur for TE/2 seconds. The formation of the echo by the 180 degree refocusing pulses is unchanged.

To isolate the peaks representing J-coupled nuclei, the TE must be set so that the J-coupling effect normally produces a 180 degree phase accumulation (resulting in inversion of the spectral peaks, see Section 4.1.2). **.** Then, two independent spectra must be acquired, one

obtained with the selective RF pulse applied to the coupled nuclei, and the other with the selective RF pulse not applied to the coupled nuclei. Subtraction of these two spectra leads to a cancellation of all spectral peaks corresponding to nuclei that were not J-coupled to the nuclei nutated by the selective RF pulse. Those peaks arising from nuclei that were J-coupled to the nuclei nutated by the selective RF pulse will be preserved, and thus their peaks can be assessed in isolation from any otherwise overlapping signal from the other nuclei.

Spectral editing for isolation of the lactate doublet at 1.32 ppm arising from the methyl protons provides an excellent example of the MEGA and BASING techniques, as shown in Figure 13. The J-coupling effect is a +-3.5 Hz change in the precession frequency. The spectral peak corresponding to the methine proton is located at 4.10 ppm on the spectrum. This separation of 2.78 ppm (355 Hz at 3.0T) permits a frequency selective RF pulse that will nutate the methine proton without affecting the methyl protons. The spectral width of the RF pulse is typically 50 Hz, so the methyl protons are not affected by the pulse centered on the methine proton, however, any protons with a resonance frequency in the range of +-25 Hertz from the methine proton will be affected by the selective pulse. During data acquisition, the J-coupling effect continues, and so the methyl protons of half the lactate molecules will show a positive change in Larmor frequency, and the methyl protons of the other half of the molecules will show a negative change. A TE of 144 ms results in an inverted doublet from the methyl protons at 1.32 ppm when no selective RF pulse is applied, while this doublet will be upright when the selective RF pulse is applied. Thus, subtraction of the former from the latter will result in a spectrum that preserves the upright doublet arising from the methyl nuclei of lactate at 1.32 ppm. Potentially overlapping signal from other nuclei (primarily lipid in this region of the spectrum) is substantially removed by the subtraction. In the case of lactate, the BASING pulse has sufficient

bandwidth that it is also used to provide water suppression, obviating the need for CHESS pulses. Although lactate is used as an example here, the same physical principles apply to spectral editing of GABA, for which MEGA-PRESS is the most commonly used pulse sequence (Mullins et al. 2014).

### 4.1.2 Spectral Editing: Correction of volume misregistration

Signal cancellation due to volume misregistration affects the measurement of J-coupled nuclei. The extent of signal cancellation increases with the magnetic field strength of the scanning system and the frequency difference between the main and the coupled nuclei. Because of this effect, peak integral values from the main nuclei (e.g. the methyl protons of lactate) are significantly reduced. Several references describe this volume misregistration effect, and it's mitigation by the addition of spectral-selective pulses with the correct timing within the PRESS sequence (Kelley et al. 1999; Sison 2006; Kaiser et al. 2007). The volume misregistration effect arises because the frequency difference between the main and the coupled nuclei influences slab selection along each of the three directions during the voxel selection process (Yablonskiy et al. 1998). As in imaging of fat versus water, the selected slice for nuclei that have a higher chemical shift value will be shifted in location, in accordance with the direction of the field gradient. This does not present a major problem with nuclei that produce singlets in the spectrum. Although each such nucleus will have a uniquely positioned voxel, the peaks arising from them are not vulnerable to signal cancellation. However, when two groups of nuclei are J-coupled, the relative shift in the location of their voxels results in loss of measured signal. At a field strength of 3.0 Tesla, for example, the resonance frequency of the lactate methine proton at 4.1 ppm is approximately 2.8 ppm (356 Hz) from the resonance frequency of the lactate methyl protons at

1.3 ppm. Since the three orthogonal slabs used for voxel definition are created using a RF pulse of 1150 Hz, the methine and methyl proton volumes are relatively shifted by about 30.9% of the voxel size in each direction. For example, if the voxel size is 40 mm in the x-direction, then the shift of the two voxels in that direction is about 12 mm. This leaves a 12 mm thick region in which the methine protons have not been inverted by the pulses, and in which the methyl protons will continue to precess in the same direction as before the pulse. Only the other 28 mm region containing the precessing methyl protons will experience the inversion of the methine protons, causing reversal of the methyl proton precession due to J-coupling. When this effect is applied to all three directions to obtain the selected voxel, the net effect is complicated and the reduction is greater than 30.9%.

Figure 14 illustrates four regions of the voxel that are generated using single voxel PRESS, when the coupled nuclei and the main nuclei have different chemical shift values. The four regions shown in this figure are generated by the two 180 degree pulses of PRESS. For the case of lactate spectroscopy using PRESS with TE 144, Figure 15 illustrates the magnetization of the methyl doublet that will be observed at TE 144 ms in each of the four regions. The evolution of the magnetization is different in each of the four regions, leading to cancellation of magnetization and reduced size of the inverted doublet. Figure 16 illustrates the magnetization of the methyl doublet when PRESS with BASING is used. With BASING pulses, the magnetization in all regions is upright and the doublet peaks are near maximal size.

A similar signal cancelation due to volume misregistration occurs with GABA editing. However, the magnitude of the effect is reduced compared to lactate because the frequency difference between the main and the coupled peak is much smaller (1.1 ppm, or 140 Hz) and thus leads to a smaller relative shift of about 12.2% of the voxel size in each direction (Edden and

Barker 2007). Recent reviews provide additional guidance with regard to MRS methods specifically targeting GABA (Mullins et al. 2014; Puts and Edden 2012).

### 4.1.3 2D NMR Spectroscopy

A more sophisticated method for separating and identifying singlets and multiplets formed by coupled nuclei groups uses a pulse sequence that resolves nuclear signals with respect to both their chemical shift and J-coupling. The output at each voxel of 2D NMR spectroscopy consists of a 2D plane of peaks, in place of the one dimensional standard spectra obtained in typical single voxel spectroscopy or CSI. In one of these pulse sequences, referred to as Correlation Spectroscopy (COSY) (Ernst et al. 1987), nuclei that are not coupled to other nuclei appear along the diagonal of the two dimensional spectral plane. Nuclei that are J-coupled appear off the main diagonal. The signals from these J-coupled nuclei appear in specific off-diagonal locations determined by the chemical shifts of the coupled nuclei groups, and the area of the peak is proportional to the number of nuclei that are contributing to that location. COSY is readily implemented for in-vivo tissue analysis (Brereton et al. 1994). The molecules contributing to complicated 1-D spectra from SVS or CSI, containing multiple overlapping peaks from the different nuclear groups that cannot be parsed to identify the individual molecules, often can be easily parsed using COSY. For more in-depth information the reader is referred to texts on 2D NMR spectroscopy and COSY in particular (Ernst et al. 1987; Rule and Hitchens 2006; Cavanagh et al. 2007; De Graaf 2007).

2D NMR spectroscopy has not been widely used in the clinical or clinical research setting, mainly because the scan times are long. The PEPSI sequence, which uses rapid frequency encoding for one dimension to eliminate one dimension of phase encoding, has been

adapted for the 2D correlated spectroscopy sequence (Lipnick et al. 2010). With this new sequence, called Echo Planar Correlated Spectroscopic Imaging (EP-COSI), the scan time can be reduced to about 20 minutes. In addition, a related sequence that is not dependent on echo-planar encoding, called Multi Echo Correlated Spectroscopic Imaging (ME-COSI), has recently been developed (Vermi et al. 2011). Further improvements in the efficiency of data acquisition in the sequence may ultimately generate reasonable scan times for clinical use (e.g <10 minutes).

### 5.1 Approaches to Quantification of MRS Metabolites

The area under a metabolite resonance in an MR spectrum is proportional to the concentration of the metabolite. Several different approaches are commonly used for quantifying the areas under metabolite resonances (Jansen et al. 2006). A traditional approach that continues to be useful for some experimental goals is peak integration. The experimenter first defines a frequency range containing the peak of interest, for example, 2.01 ± 0.15 ppm for the NAA peak (Figure 1). Then, summing the values across that frequency range and subtracting an estimate of the baseline above which the peak arises, calculate the area under the curve. This method is not useful for quantifying overlapping peaks. Peak integration is more suitable for longer TE sequences, which have less complex baselines and fewer overlapping peaks than short TE sequences (Figure 1). Similarly, peak integration can also be useful for quantifying J-edited peaks in difference spectra.

Peak fitting methods can provide more accurate quantification of the metabolite signal intensity than peak integration for many experimental situations. With these methods, each important peak in the spectrum is fitted to a model peak shape defined mathematically, for which the fitted peak has a known value for its integral (i.e. its area under the curve). Then an optimal

combination of peak integral values is iteratively calculated for the entire set of peaks. This method is most useful when combined with prior knowledge about the metabolite signals giving rise to the spectrum. Such prior knowledge can include frequency relationships, amplitude ratios, scalar coupling and other features that are known to be characteristic of the peaks arising from a specific metabolite. The prior knowledge approach is used in the AMARES (Advanced Method for Accurate Robust and Efficient Spectral fitting) program incorporated into the Magnetic Resonance User Interface (MRUI) software package (MRUI 2009). The most comprehensive approach to using prior knowledge involves using simulated or empirical metabolite basis sets. This approach is used in the LCModel (Linear Combination Model) software, which is a widely used commercially available package (Provencher 1993), and in the QUEST (quantitation based on Quantum ESTimation) program incorporated into the MRUI software package (MRUI 2009). Using these methods requires simulating or measuring (*in vitro* using phantoms) the specific response of every anticipated metabolite to the exact scanning parameters used. With this method, information about relaxation times, chemical shifts, peak splitting patterns, J-evolution, etc. matches the *in vivo* conditions and is available for model estimation. The information for each metabolite informs the basis set that constrains the iterative peak fitting calculations used for quantifying signal intensity values for metabolites in the experimental, *in vivo* MRS data.

An important limitation of whole-body MR systems used in diagnostic imaging is that there is no attempt by the system to hold fixed or measure the scaling factor between the measured raw data values and the strength of the magnetization giving rise to those values. Because this scaling factor is unknown and variable across subjects and brain regions, the raw signal intensity values for each measurement cannot be easily converted to absolute concentration values (e.g. moles per cc of tissue). Two general approaches are typically used to

control for variability in this scaling factor: 1) relative quantification; and 2) estimated absolute quantification. Each of these approaches has advantages and disadvantages. The choice of which approach to use may vary depending upon the circumstances and goals of a particular MRS experiment. General features of the two approaches are discussed below.

### 5.1.1 Relative Quantification of MRS metabolites

The most widely used method of relative quantification in brain 1H-MRS experiments is ratio normalization using an endogenous metabolite. With this approach, the signal intensity values from each metabolite of interest in a given 1H-MRS acquisition are normalized to the signal value of a reference metabolite measured simultaneously in the same voxel. Because it is a strong signal with relatively low variability across brain regions and across subjects, total creatine (creatine plus phosphocreatine) is most commonly used as the reference metabolite in this method of ratio normalization (de Graaf 2007). Ratio normalization using the creatine signal value is referred to as creatine normalization. Since the unknown scaling factor in effect for a given 1H-MRS acquisition influences the signal from each metabolite within the voxel equally, creatine normalization reduces the variance due to that factor. For any given MRS acquisition, cerebrospinal fluid (CSF) constitutes a variable proportion of the total volume of the voxel. Since the proportion of CSF within the voxel affects the measured signal similarly for each parenchymal metabolite, the creatine normalization procedure is also a useful way to correct for variation due to this partial volume effect.

The most important disadvantage of creatine normalization derives from the fact that creatine concentration varies across subjects. In the best case, this variation across subjects is random with respect to the subject groups of interest for a specific MRS experiment. In this case,

creatine variation adds to the overall variance in the data when creatine normalization is used. A more serious problem occurs when there is a systematic difference in creatine concentration between two groups of subjects. In this case, the creatine normalization approach may lead to false positive or false negative findings. For example, the NAA/creatine ratio may be similar between two groups, but both NAA and creatine may actually be reduced in one group. Alternatively, the NAA/creatine ratio may be significantly higher in one group, but this may be due primarily to decreased creatine in that group, rather than increased NAA. The likelihood that differences in creatine values are confounding group differences in creatine normalized data is diminished when many creatine normalized metabolites are compared across groups, but only one metabolite is observed to be abnormal. In schizophrenia, the psychiatric disorder most extensively studied with 1H-MRS, there is no consistent evidence for abnormalities in brain creatine concentrations (Deicken et al. 2000). The potential for confounding effects of systematic differences in creatine values is also reduced in dynamic 1H-MRS studies, in which repeated measures are made in the same subject before and after an experimental manipulation (e.g. neural activation). Since total creatine values appear to be stable over short term repeated measurements, dynamic changes in a creatine-normalized metabolite (e.g. lactate/creatine ratio) are unlikely to be due to changes in creatine.

### 5.1.2 Estimated Absolute Concentrations using Internal Water

The primary alternative to creatine normalization or other relative quantification approaches is normalizing metabolite signal values to the water signal measured in the same voxel (de Graaf 2007; Ernst et al. 1993; Malucelli et al. 2009). This approach requires at least two additional steps during the acquisition of the 1H-MRS data, and additional calculations during post-

processing of the data. The procedure can generate an estimated absolute concentration for each metabolite in the voxel, but it relies on measurement of the partial volumes of gray matter, white matter and CSF within the voxel. A significant challenge to the accuracy of partial volume measurements is achieving precise registration of the voxel to the high-resolution anatomical images. This method also assumes canonical values for the concentration of water in gray matter, white matter, and CSF, which assumes that tissue water concentrations do not vary across subjects. The most common implementation of this method also relies on canonical values for the relaxation times of brain water and metabolites, again assuming no differences between subject groups. Use of this approach requires collecting an additional 1H-MRS acquisition using the same scanning parameters applied during collection of the metabolite data, except that the water suppression pulses are omitted. This water non-suppressed acquisition provides a measure of the full water signal from the voxel. In addition, it is necessary to acquire a structural MR image of the tissue within the voxel with good contrast between gray matter, white matter, and CSF. After coregistration, this image is used to segment the voxel into gray matter, white matter and CSF partial volumes (Gasparovic et al. 2006; Gussew et al. 2012).

First, the concentration of water in the voxel is estimated from the results of the tissue segmentation analysis of the voxel, as follows:

$$C_{water} = (F_{gm}*C_{gm}) + (F_{wm}*C_{wm}) + (F_{csf}*C_{csf})$$

where $C_{water}$ is the overall concentration of water in the voxel, $F_{gm}$ is the fraction of the voxel composed of gray matter, $C_{gm}$ is the canonical value for the concentration of water in gray matter (43.30 molar), $F_{wm}$ is the fraction of the voxel composed of white matter, $C_{wm}$ is the canonical value for the concentration of water in white matter (36.08 molar), $F_{csf}$ is the fraction of the voxel

composed of CSF, $C_{csf}$ is the canonical value for the concentration of water in CSF (55.51 molar) (Malucelli et al. 2009; Minati et al. 2010).

Then, the estimated concentration of water in the voxel and the water signal intensity acquired from the voxel are used to estimate the scaling factor. Along with corrections for number of protons giving rise to each signal and corrections for relaxation time effects, the estimated concentration of the metabolite in the voxel is calculated as follows:

$$C_{met} = [S_{met}(0)/S_{water}(0)] * N_{water}/ N_{met}$$

where $C_{met}$ is the concentration of the metabolite in the voxel, $S_{met}(0)$ is the metabolite signal extrapolated to TE = 0, $S_{water}$ (0) is the water signal extrapolated to TE = 0, $N_{water}$ is the number of protons giving rise to the water signal (2), and $N_{met}$ is the number of protons giving rise to the metabolite signal (Malucelli et al. 2009).

The correction to be used for relaxation times can be taken from published values (Frahm et al. 1989a; Kreis et al. 1993; Kreis 1997; Mlynárik et al. 2001; Träber et al. 2004; Jansen et al. 2006) or it can be empirically measured in the same subjects. However, measurement of relaxation times requires considerable additional scanning time and is rarely done. Relaxation time corrections can be applied using different values for the gray matter, white matter and CSF partial volumes or they can be applied with a single value for the whole voxel (Malucelli et al. 2009; Minati et al. 2010). In some experiments, it may be appropriate to normalize the metabolite concentration to the fraction of brain tissue (gray matter plus white matter) in the voxel ($1-F_{csf}$).

### 5.1.3 Estimated Absolute Concentrations using Phantom Calibration

Another approach to estimating the absolute concentrations of metabolites involves the use of a phantom containing a known concentration of a reference metabolite, such as creatine (Soher et al. 1996; Jansen et al. 2006). There are two approaches to calibration with a phantom, referred to as "in-place" and "in-time". The "in-time" approach requires one or more small cylindrical phantoms that are placed alongside the patient's head during the spectroscopy scan. Because the sensitivity of the RF receiver coil, and thus the overall scaling factor, is dependent on the location of the voxel, in-time approach is imprecise and has not been widely used for calibration of MR spectra. The "in-place" approach acquires MR spectra from the phantom immediately after the spectroscopy scan has been run on the patient. The phantom is substituted for the patient and the MR spectroscopy scan is rerun, using the same voxel location. The scaling factor for that voxel location can then be calculated from the ratio of the metabolite peak integral with known metabolite concentration in the phantom. This can be used to scale the metabolite peak integral from the patient. However, when the phantom replaces the patient in the scanner, the main magnetic field must be reshimmed to provide sharp peaks in the phantom spectra. The calibration of peak integrals in the patient based on those observed in the phantom is valid provided that no change in the receiver sensitivity or other scaling factors has occurred. The reshimming of the main magnetic field required when the phantom replaces the patient in the scanner is sometimes associated with changes in scaling factors. Care must be taken that this does not occur.

Soher and colleagues (Soher et al. 1996) have described an important source of difference in the scaling factors between the phantom and the patient that limits the accuracy of the "in place" phantom calibration technique. The signal intensity generated in the RF coil by a given magnetization in the object within the coil will vary as a function of the dielectric load of the

object on the receiver coil. The dielectric load of the phantom may differ substantially from the dielectric load of the patient. In general, the higher the dielectric load, the smaller the magnetic field reaching the coil and the smaller the voltage induced in the coil. According to the reciprocity theorem (Chen and Hoult 1989), the dielectric load of the object affecting the magnetic field from the voxel can be measured using the transmit voltage setting of the RF transmitter needed to nutate the magnetization in that same voxel. A larger transmit voltage indicates a greater loss of magnetic field within the object during nutation. The reciprocity theorem states that same relative loss of field will occur when the magnetic field generated by magnetization inside the brain extends outside the brain to the coil. This effect is taken into account by scaling the peak integrals in proportion to the inverse of the transmit voltage. Including this scale factor on the peak integrals has been shown to improve the agreement between measured peak integrals and actual known concentrations of metabolites in phantom.

It is important to emphasize that the reciprocity theorem is not applicable when the RF coil used for transmission is not the same as the coil used for reception. The mathematical relationship between the attenuation of the received signal from the voxel, and the transmit voltage needed to nutate the magnetization of the same voxel, exists only if the same coil is used for transmission and reception. However, the use of the same coil for transmission and reception is becoming less common. Modern multi-element coils provide spectra with the highest SNR, but they are designed only for signal reception. These coils are not able to provide transmit RF fields for nutation of the magnetization. Consequently, the body coil is typically used for transmission. Alternatively, a standard quadrature head coil can be used for both transmission and reception, as was done by Soher and colleagues (Soher et al. 1996) demonstrating this calibration technique. However, the SNR of a quadrature transmit/receive head coil is much

lower than that of a multi-element head coil. The requirement to use a transmit/receive head coil will limit the use of this refinement of the "in place" phantom calibration technique.

### 6.1 Conclusions

Magnetic resonance spectroscopy can provide *in vivo* neurochemical information about the metabolic and information processing infrastructure of the brain that is not accessible by any other means using currently available experimental methods. The physical instrumentation, pulse sequences, and post-processing methods for MRS are continually improving, enabling reliable measurement of an expanding set of important brain metabolites. The physical principles underlying MRS are distinct in many ways from those underlying magnetic resonance imaging and may be unfamiliar to cognitive, behavioral, and clinical neuroscientists who are considering the use of MRS in their experimental designs. It is hoped that the physical principles and technical methods reviewed here will assist such investigators in making optimal choices in the selection of pulse sequences and post-processing methods that will best support their research goals.

**References**

Adalsteinsson, E., Irarrazabal, P., Topp, S., Meyer, C., Macovski, A. and Spielman, D.M. (1998). Volumetric spectroscopic imaging with spiral-based k-space trajectories. Magn Reson Med *39*, 889–898.

Allen, P.S. and Thompson, R.B. (1999). On the localized quantification of metabolites with coupled spins. MAGMA *9*, 159-163.

Bhattacharyya, P.K., Lowe, M.J., and Phillips, M.D. (2007). Spectral quality control in motion-corrupted single-voxel J-difference editing scans: an interleaved navigator approach. Magn Reson Med *58*, 808-812.

Bogner, W., Hess, A.T., Gagoski, B., Tisdall, M.D., van der Kouwe, A.J., Trattnig, S., Rosen, B. and Andronesi, O.C. (2013). Real-time motion- and B0-correction for LASER-localized spiral-accelerated 3D-MRSI of the brain at 3T. Neuroimage *88*, 22-31.

Bottomley, P.A. (1984). Selective volume method for performing localized NMR spectroscopy. In, vol #4480228. General Electric Company, USA.

Bottomley, P.A. (1987). Spatial localization in NMR spectroscopy in vivo. Ann NY Acad Sci *508*, 333-348.

Brereton, M., Galloway, G.J., Rose, S.E. and Doddrell, D.M. (1994). Localized two-dimensional shift correlated spectroscopy in humans at 2 Tesla. Magn Reson Med *32*, 251-7.

Cavanagh, J., Fairbrother, W.J., Palmer, A.G., Rance, M., and Skelton, N.J. (2007). Protein NMR Spectroscopy: Principles and Practice (Burlington, MA, USA: Elsevier Academic Press).

Chen, C.N. and Hoult, D.L. (1989). Biomedical Magnetic Resonance Technology (New York, NY, USA: Adam Hilger Publishing).

De Graaf, R.A. (2007). In-vivo NMR Spectroscopy: Principles and Techniques (Chichester, UK: John Wiley & Sons).

Dean, J.A. (1992). Lange's Handbook of Chemistry (New York, NY, USA: McGraw-Hill, Inc.).

Edelman, R.R. (2006). Clinical Magnetic Resonance Imaging (Philadelphia, PA, USA: Saunders Elsevier).

Deicken, R.F., Johnson, C., and Pegues, M. (2000). Proton magnetic resonance spectroscopy of the human brain in schizophrenia. Rev Neurosci *11*, 147–158.

Edden, R.A.E., and Barker, P.B. (2007). Spatial effects in the detection of gamma- aminobutyric acid: Improved sensitivity at high fields using inner volume saturation. Magn Reson Med *58*, 1276–82.

Ernst, R.R., Bodenhausen, G., and Wokaun, A. (1987). Principles of Nuclear Magnetic Resonance in One and Two Dimensions (Oxford, UK: Clarendon Press).

Ernst, T. and Chang, L. (1996). Elimination of artifacts in short echo time 1H MR spectroscopy of the frontal lobe. Magn Reson Med *36*, 462–468.

Ernst,T. and Hennig, J. (1991). Coupling effects in volume selective 1H spectroscopy of major brain metabolites. Magn Reson Med *21*, 82-96.

Ernst, T., Kreis, R. and Ross, B.D. (1993). Absolute quantitation of water and metabolites in the human brain. I. Compartments and water. J Magn Reson *102*, 1–8.

Frahm, J., Bruhn, H., Gyngell, M.L., Merboldt, K.D., Hänicke, W., Sauter, R. (1989a). Localized proton NMR spectroscopy in different regions of the human brain in vivo: Relaxation times and concentrations of cerebral metabolites. Magn Reson Med *11*, 47-63.

Frahm, J., Bruhn, H., Gyngell, M.L., Merboldt, K.D., Hänicke, W. and Sauter, R. (1989b). Localized high-resolution proton NMR spectroscopy using stimulated echoes: initial applications to human brain in vivo. Magn Reson Med. *9*, 79-93.

Garwood, M. and DelaBarre, L. (2001). The return of the frequency sweep: designing adiabatic pulses for contemporary NMR. J. Magn. Reson., *153*, 155–177.

Gasparovic, C., Song, T., Devier, D., Bockholt, H.J., Caprihan, A., Mullins, P.G., Posse, S., Jung, R.E. and Morrison, L.A. (2006). Use of tissue water as a concentration reference for proton spectroscopic imaging. Magn Reson Med. *55*, 1219-26.

Gautreau, R. and Savin, W. (1978). Theory and Problems of Modern Physics (New York, NY, USA: McGraw-Hill).

General_Electric (1999). Operator Manual for SIgna Horizon LX and Signa MR/I Systems: Multi-Nuclear Spectroscopy Features, Operating Documentation, Release 8.3.

Govindaraju, V., Young, K., and Maudsley, A.A. (2000). Proton NMR chemical shifts and coupling constants for brain metabolites. NMR Biomed *13*, 129-153.

Gussew, A., Erdtel, M., Hiepe, P., Rzanny, R. and Reichenbach, J.R. (2012). Absolute quantitation of brain metabolites with respect to heterogeneous tissue compositions in (1)H-MR spectroscopic volumes. MAGMA. *25*, 321-33.

Haacke, E.M., Brown, R.W., Thompson, M.R., and Venkatesan, R. (1999). Magnetic Resonance Imaging: Physical Principles and Sequence Design ((New York, NY, USA: Wiley-Liss).

Haase, A., Frahm, J., Hanicke, W., and Matthaei, D. (1985). H-1 NMR chemical shift selective (CHESS) imaging. Phys Med Biol *30*, 341-344.

Hancu, I., and Port, J. (2011). The case of the missing glutamine. NMR Biomed *24*, 529–35.

Harris, A.D., Glaubitz, B., Near, J., Evans, C.J., Puts, N.A.J., Schmidt-Wilcke, T., Tegenthoff, M., Barker, P.B. and Edden, R.A.E. (2014). Impact of frequency drift on gamma-aminobutyric acid-edited MR spectroscopy. Magn Reson Med *72*, 941–948.

Hetherington, H.P., Avison, M.J., and Shulman, R.G. (1985). 1H homonuclear editing of rat brain using semiselective pulses. Proc Natl Acad Sci U S A *82*:3115-3118.

Jansen, J.F., Backes, W.H., Nicolay, K., and Kooi, M.E. (2006). 1H MR spectroscopy of the brain: absolute quantification of metabolites. Radiology *240*, 318-332.

Kaiser, L.G., Young, K., and Matson, G.B. (2007). Elimination of spatial interference in PRESS-localized editing spectroscopy. Magn Reson Med *58*, 813-818.

Keating, B., Deng, W., Roddey, J.C., White, N., Dale, A., Stenger, V.A. and Ernst, T. (2010). Prospective motion correction for single-voxel 1H MR spectroscopy. Magn Reson Med *64*: 672-679.

Kelley, D.A., Wald, L.L., and Star-Lack, J.M. (1999). Lactate detection at 3T: compensating J coupling effects with BASING. J Magn Reson Imaging *9*, 732-737.

Kohler, S. (1993). PROBE/SV: Signal-voxel Proton Brain Exam Applications Guide. Signa Applications Guide, Catalog No. E8804DD, MR Advanced Applications. GE Medical Systems, Milwaukee, WI.

Kreis, R. (1997). Quantitative localized 1H MR spectroscopy for clinical use. Prog Nucl Magn Reson Spectroscopy *31*, 155-195.

Kreis, R., Ernst, T., and Ross, B.D. (1993). Development of the human brain: in vivo quantification of metabolite and water content with proton magnetic resonance spectroscopy. Magn Reson Med *30*, 424-437.

Lange, T., Zaitsev, M. and Buechert, M. (2011). Correction of frequency drifts induced by gradient heating in 1H spectra using interleaved reference spectroscopy. J Magn Reson Imaging *33*, 748–754.

Levitt, M.H. (2008). Spin Dynamics: Basics of Nuclear Magnetic Resonance (Chichester, UK: John Wiley & Sons, Ltd.).

Lipnick, S., Verma, G., Ramadan, S., Furuyama, J., and Thomas, M.A. (2010). Echo Planar Correlated Spectroscopic Imaging (EP-COSI): Implementation and Pilot Evaluation in Human Calf in Vivo Magn Reson Med *64*, 947-956.

Maddock, R.J. and Buonocore, M.H. (2008). Measuring brain lactate at rest and during visual

stimulation. Psychiatry Res Neuroimaging *162*, 175-179.

Maddock, R.J. and Buonocore, M.H. (2012). MR spectroscopic studies of the brain in psychiatric disorders. Current Topics in Behavioral Neuroscience, *11*, 199-251.

Maddock, R.J., Buonocore, M.H., Lavoie, S.P., Copeland, L.E., Kile, S.J., Richards, A.L., and Ryan, J.M. (2006). Brain lactate responses during visual stimulation in fasting and hyperglycemic subjects: a proton magnetic resonance spectroscopy study at 1.5 Tesla. Psychiatry Res *148*, 47-54.

Malucelli, E., Manners, D.N., Testa, C., Tonon, C., Lodi, R., Barbiroli, B., and Iotti, S. (2009). Pitfalls and advantages of different strategies for the absolute quantification of N-acetyl aspartate, creatine and choline in white and grey matter by 1H-MRS. NMR Biomed *22*, 1003-1013.

Mescher, M., Merkle, H., Kirsch, J., Garwood, M., and Gruetter, R. (1998). Simultaneous in vivo spectral editing and water suppression. NMR Biomed *11*, 266-272.

Mescher, M., Tannus, A., Johnson, M.O., and Garwood, M. (1996). Solvent suppression using selective echo dephasing. J Magn Reson A *123*, 226-229.

Minati, L., Aquino, D., Bruzzone, M.G., and Erbetta, A. (2010). Quantitation of normal metabolite concentrations in six brain regions by in-vivoH-MR spectroscopy. J Med Phys *35*, 154-163.

Mlynárik, V., Gambarota, G., Frenkel, H. and Gruetter, R. (2006). Localized short-echo-time proton MR spectroscopy with full signal-intensity acquisition. Magn Reson Med *56*, 965-70.

Mlynárik, V., Gruber, S., and Moser, E. (2001). Proton T (1) and T (2) relaxation times of human brain metabolites at 3 Tesla. . NMR Biomed *14*, 325-331.

MRUI (2009). Magnetic Resonance User Interface. Accessed July 2011. Available at http://www.mrui.uab.es/mrui/mrui_Overview.shtml.

Mullins, P. G., McGonigle, D. J., O'Gorman, R. L., Puts, N. A. J., Vidyasagar, R., Evans, C. J., Cardiff Symposium on MRS of GABA, and Edden, R.A. (2014). Current practice in the use of MEGA-PRESS spectroscopy for the detection of GABA. NeuroImage. *86*, 43-52.

Ogg, R.J., Kingsley, P.B. and Taylor, J.S. (1994). WET, a T1- and B1-insensitive water-suppression method for in vivo localized 1H NMR spectroscopy. J Magn Reson B. *104*, 1-10.

Posse, S., Dager, S.R., Richards, T.L., Yuan, C., Ogg, R., Artru, A.A., Müller-Gärtner, H.W., and Hayes, C. (1997). In vivo measurement of regional brain metabolic response to hyperventilation using magnetic resonance: proton echo planar spectroscopic imaging (PEPSI). Magn Reson Med *37*, 858-865.

Posse, S., Tedeschi, G., Risinger, R., Ogg, R. and Le Bihan, D. (1995). High speed 1H spectroscopic imaging in human brain by echo planar spatial-spectral encoding. Magn Reson Med *33*, 34-40.

Provencher, S.W. (1993). Estimation of metabolite concentrations from localized in vivo proton NMR spectra. Magn Reson Med *30*, 672–679.

Puts, N. A. J. and Edden, R. A. E. (2012). In vivo magnetic resonance spectroscopy of
GABA: a methodological review. Prog Nucl Magn Reson Spectroscopy *60*, 29–41.

Rae, C. D. (2014). A guide to the metabolic pathways and function of metabolites observed in human brain (1)H magnetic resonance spectra. Neurochem Res, *39*, 1–36.

Rule, G.S. and Hitchens, K.T. (2006). Fundamentals of Protein NMR Spectroscopy (Dordrecht, The Netherlands: Springer).

Schubert, F., Gallinat, J., Seifert, F., and Rinneberg, H. (2004). Glutamate concentrations in

human brain using single voxel proton magnetic resonance spectroscopy at 3 Tesla. NeuroImage *21*, 1762–71.

Siemens (2004). MR Spectroscopy Quick Guide for MAGNETOM Trio. Solutions. Siemens AG, Munchen, Germany.

Siemens ( 2002). MR Spectroscopy Manual, Version syngo MR 2002B. SMEGM. Siemens AG Erlangen, Germany.

Sison, S. (2006). Magnetic Resonance Spectroscopy Sequence Development for Optimal Lactate Detection. Thesis in Biomedical Engineering. University of California Davis, Davis, p 91.

Soher, B.J., van Zijl, P.C., Duyn, J.H., and Barker, P.B. (1996). Quantitative proton MR spectroscopic imaging of the human brain. Magn Reson Med *35*, 356-363.

Star-Lack, J., Nelson, S.J., Kurhanewicz, J., Huang, L.R., and Vigneron, D.B. (1997). Improved water and lipid suppression for 3D PRESS CSI using RF band selective inversion with gradient dephasing (BASING). Magn Reson Med *38*, 311-321.

Star-Lack, J., Spielman, D., Adalsteinsson, E., Kurhanewicz, J., Terris, D.J., and Vigneron, D.B. (1998). In vivo lactate editing with simultaneous detection of choline, creatine, NAA, and lipid singlets at 1.5 T using PRESS excitation with applications to the study of brain and head and neck tumors. J Magn Reson *133*, 243-254.

Terpstra, M., Henry, P.G., and Gruetter, R. (2003). Measurement of reduced glutathione (GSH) in human brain using LCModel analysis of difference-edited spectra. Magn Reson Med *50,* 19-23.

Thompson, R.B. and Allen, P.S. (1999). Sources of variability in the response of coupled spins to the PRESS sequence and their potential impact on metabolite quantification. Magn Reson Med *41*, 1162-1169.

Thompson, R B, and Allen, P.S. (2001). Response of metabolites with coupled spins to the STEAM sequence. Magn Reson Med *45*, 955–65.

Tkác, I., Starcuk, Z., Choi, I.Y. and Gruetter, R. (1999). In vivo 1H NMR spectroscopy of rat brain at 1 ms echo time. Magn Reson Med *41*, 649-56.

Tofts, P. and Waldman, A.D. (2003). Chapter 9, Spectroscopy: 1H Metabolite Concentrations. Quantitative MRI of the Brain: Measuring Changes Caused by Disease. Tofts, P., ed. (West Sussex, UK: John Wiley & Sons), pp 299-340.

Träber, F., Block, W., Lamerichs, R., Gieseke, J., and Schild, H.H. (2004). 1H metabolite relaxation times at 3.0 Tesla: Measurements of T1 and T2 values in normal brain and determination of regional differences in transverse relaxation J Magn Reson Imaging *19*, 537-545.

Verma, G., Lipnick, S., Ramadan, S., Nagarajan, R., and Thomas, M. A. (2011). Implementation of multi-echo-based correlated spectroscopic imaging and pilot findings in human brain and calf muscle. J Magn Reson Imaging *34*, 262–269.

Yablonskiy, D.A., Neil, J.J., Raichle, M.E., and Ackerman, J.H. (1998). Homonuclear J coupling Effects in Volume Localized NMR Spectroscopy: Pitfalls and Solutions. Magn Reson Med *39*, 169-178.

## Table: Nuclei for clinical MRS

| Nucleus | Name | Intrinsic spin (*I*) | Magnetic moment (units of nuclear magneton) | Gyro-magnetic ratio (MHz/T) | Larmor frequency at 1.5 tesla (MHz) | Inherent sensitivity per nucleus (relative to $^{1}H$) | Natural abundance of nucleus (%) | Inherent sensitivity per element (relative to $^{1}H$) |
|---|---|---|---|---|---|---|---|---|
| $^{1}H$ | Hydrogen (proton) | 1/2 | 2.793 | 42.58 | 63.86 | 1.000 | 99.985 | 1.00 |
| $^{23}Na$ | Sodium | 3/2 | 2.218 | 11.26 | 16.89 | 0.0925 | 100.0 | $9.25 \times 10^{-2}$ |
| $^{31}P$ | Phosphorus | 1/2 | 1.132 | 17.24 | 25.86 | 0.0664 | 100.0 | $6.64 \times 10^{-2}$ |
| $^{13}C$ | Carbon | 1/2 | 0.7024 | 10.72 | 16.06 | 0.0160 | 1.108 | $1.77 \times 10^{-4}$ |
| $^{14}N$ | Nitrogen | 1 | 0.4038 | 3.076 | 4.61 | 0.00101 | 99.63 | $1.00 \times 10^{-3}$ |
| $^{15}N$ | Nitrogen | 1/2 | -0.2832 | -4.315 | -6.473 | 0.00104 | 0.367 | $3.82 \times 10^{-6}$ |
| $^{17}O$ | Oxygen | 5/2 | -1.894 | -5.772 | -8.658 | 0.0291 | 0.0038 | $1.10 \times 10^{-6}$ |
| $^{39}K$ | Potassium | 3/2 | 0.3915 | 1.987 | 2.981 | 0.00051 | 93.26 | $4.74 \times 10^{-4}$ |
| $^{19}F$ | Fluorine | 1/2 | 2.629 | 40.06 | 60.09 | 0.833 | 100 | $8.33 \times 10^{-1}$ |

Values are from (Dean 1992). The value of the nuclear magneton unit is 5.059 x 10^-27 Joules/Tesla. MHz/T is megaHertz per Tesla. Inherent sensitivity refers to the sensitivity for detection of a single nucleus in an MRS experiment. It is a function of the intrinsic spin and the gyromagnetic ratio and is calculated relative to the value for hydrogen. Natural abundance of nucleus refers to the percentage of the listed isotope among all of the isotopes of that element. Inherent sensitivity per element takes into account the natural abundance of the indicated isotope, relative to all of the isotopes of the element.

**Figure legends**

**Figure 1**: Representative 1H-MRS spectra acquired from human brain using three different TEs. The spectrum in (A) was acquired at TE = 30 ms from the anterior cingulate cortex at 3 Tesla. The spectra in (B and C) were acquired at TE = 144 and 288 ms respectively from the primary visual cortex at 1.5 Tesla. Selected metabolite peaks are indicated. Note that the ppm value on the horizontal axis increases to the left, not the right. Spectral peaks that appear on the right side of the graph arise from nuclei that are relatively more shielded from the main magnetic field by nearby electrons. Spectral peaks on the left side of the graph arise from relatively less shielded nuclei (discussed in section in 1.2.1).

**Figure 2:** Single voxel MRS spectra with varying line widths were obtained using the PRESS Sequence (TE/TR = 144/2000 ms) on a 1.5 T system. The peaks for NAA, creatine (Cr1 and Cr2), and choline (Cho) are shown. Panels A through D illustrate a range of line widths from narrow to broad. When the line width is narrow, variation in line width is mainly related to the transverse relaxation time (T2) of the magnetization giving rise to the signal. A longer T2 leads to a narrower line width. Line width is also directly related to the inhomogeneity of the main magnetic field within the volume of the defined voxel. Greater inhomogeneity causes a broadening of the line width and a reduction in the signal to noise ratio (SNR). Lower SNR is reflected in the larger signal variations of the spectral baseline and peaks, as illustrated in spectrum D. The line widths (full width at half maximum) in ppm and Hz are: A) 0.0485 ppm, 3.10 Hz, B) 0.0680 ppm, 4.34 Hz, C) 0.136 ppm, 8.68 Hz, D) 0.165 ppm, 10.54 Hz.

**Figure 3:** The lactate molecule is depicted with carbon atoms shown in black, oxygen in red, and hydrogen in white. The proton of the methine (C-H) group (identified with dotted circle) neighbors an oxygen atom, which decreases the electron density around the proton. Hence the shielding of that proton is relatively weak, and the signal on the MR spectrum appears on the left side of the standard spectrum (at 4.1 ppm). The protons of the methyl group (identified with dashed circles) are distant from the "electron withdrawing" oxygen atom. Thus, their electron density is relatively high and the shielding is greater. These protons give rise to a signal on the right side of the standard spectrum (at 1.32 ppm). In lactate, the methine proton is J-coupled to the three methyl group protons through the C-C bond between them. The coupling causes the precession frequency of the protons in one group to be shifted, in accordance with the quantum state of the protons in the other group. In lactate, the shift in precession frequency is ±3.47 Hz (J = 6.93 Hz). The effect of this coupling is illustrated schematically in Figure 5.

**Figure 4:** J-coupling effect of nucleus X on nucleus A. In the J-coupling most prevalent in in-vivo 1H-MRS, the A and X nucleus are covalently attached to carbon atoms, which are covalently bonded to each other. The Larmor frequency of the A nucleus, in the absence of J-coupling, is denoted by $\delta_A$ on the ppm scale of the horizontal axis. With J-coupling, the Larmor frequency of A is affected by the spin state of the X nucleus. If the X nucleus is spin up (as shown on right side of the figure), the J-coupling decreases the Larmor frequency by the amount J/2. If this X nucleus is spin-down (as shown on the left side), the J-coupling increases the Larmor frequency by the amount J/2. Because nucleus A is J-coupled to only one nucleus, the signal from nucleus A in all of the molecules is split into only two peaks.

**Figure 5:** J coupling effect in the Lactate molecule: A) the effect of the methine proton X on the signal from the three methyl group protons A1, A2, A3, generates a doublet; B) the effect of three methyl group protons (labeled A1, A2 and A3) on the signal from the methine proton (labeled X), generates a quartet. Relatively high electron shielding around the methyl group protons places the center of the doublet at 1.32 ppm (see Figure 3). Relatively low electron shielding around the methine group protons places the center of the quartet at 4.1 ppm. Because of rapid rotation of the bond linking the methyl and methine groups, the methyl protons are equivalent in their interaction with the methine group proton. In A, when the methine proton is spin down, the Larmor frequency of the three methyl protons are each equivalently increased by 1/2 J. When the methine proton is spin-up, the Larmor frequency of the methyl proton is decreased by J/2. Because the probability of any particular methine proton being spin-down or spin-up is 50-50, the relative areas of these peaks are in the ratio 1 to 1. In B, the Larmor frequency of the methine proton X is shifted in accordance with the number of methyl protons that are spin-up and spin-down. When all three methyl protons A1, A2, and A3 are spin down, the Larmor frequency of the methine proton X is increased by 3/2 J. When two methyl protons are spin-down and one is spin-up, the Larmor frequency of the methine proton is increased by J/2, and when one methyl proton is spin-down and two are spin-up, the Larmor frequency of the methine proton is decreased by J/2. Finally, if all three protons are spin up, the Larmor frequency of proton X is decreased by 3/2 J. Because the probability of any particular methyl proton being spin-down or spin-up is 50-50, the relative areas of these peaks are in the proportion 1 to 3 to 3 to 1, respectively.

**Figure 6:** Sequence of RF and gradient pulses used for voxel selection in the PRESS

spectroscopy sequence. The RF line shows the radiofrequency pulses applied, and the x, y and z lines show the x, y and z gradient pulses, respectively. When RF pulses and gradient pulses are applied simultaneously, a slice of excited spins is created. The application of successive RF pulses with x, y and z gradients leads to a voxel with magnetization that refocuses and forms a spin echo at a definite time after the last 180 pulse (defined as the echo time, TE). The light blue, dark blue and red regions shown in each successive pulse identify the voxels that are defined at each stage of the selection process. The red region corresponds to the final voxel, which will provide the signal at TE and during the data acquisition period after the echo formation.

**Figure 7:** Timing of the 90-180-180 degree RF pulses in the PRESS sequence. The diagonal lines represent the phase progression of representative magnetization vectors at different locations within the final voxel. These evolve differently due to the underlying B0 magnetic field, but they are refocused by the 180 degree pulses of the PRESS sequence. By separating the 180 degree pulses by TE/2, refocusing of the magnetization vectors to produce the echo will occur at time TE after the initial 90 degree excitation pulse. The time $\Delta t$ between the 90 and 180 degree pulses does not affect the TE, and is usually chosen as short as possible consistent with the duration requirements of the gradient pulses.

**Figure 8:** Pulse sequence diagram for the CSI sequence, which combines the voxel selection process of PRESS with phase encoding for creating resolution voxels within the excitation voxel defined by the PRESS sequence. The lines within the diamond shaped features, on the x-Gradient line (B) and the y- Gradient line (B), indicate the phase encoding steps of the gradients that are applied successively in each TR period. To create a 2D grid of resolution voxels, all

combinations of phase encoding steps must be run. For example, to create an 8 x 8 grid of resolution voxels, 64 combinations of x-Gradient and y-Gradient phase encode steps must be played out, over 64 TR periods. Other items in the picture are (A) representation of water suppression pulses, (D) z- Gradient, which includes a gradient pair placed before and after the first 180 degree pulse to sharpen the edges of the voxel, and a pulse applied during the second 180 degree pulse to complete the final voxel definition, and (E), the signal (called the Free Induction Decay (FID)), starting at the TE.

**Figure 9:** The figure shows the 16 x 16 phase encoding grid, the 8 x 10 sub-grid for computing spectra, and the boundary for automatic magnetic field shimming, for a 2D CSI experiment. The figure also shows spectra computed by the MR system software, in picture icon form. The yellow boundary indicates the user-defined region that is partitioned into a user-defined grid of resolution voxels (here 16 x 16) shown in green. The blue line indicates the user-specified excitation voxel, where spectral data will be acquired for each enclosed resolution voxel. The blue line also defines the region that will be shimmed by the MR system. Note that the spatial extent of the resolution voxels is much greater than the spatial extent of the excitation voxel. This prevents artifact from spurious signal originating outside the excitation voxel through the phase encoding wrap-around artifact. Spatial saturation pulses (not shown) are applied outside of the region of the solid blue line to suppress spurious signal from outside the excitation volume.

**Figure 10:** Pulse sequence diagram for the Chemical Shift Selective Suppression (CHESS) module for water suppression. The CHESS module consists of three RF pulses followed by large amplitude and duration gradient pulses. The net effects of these pulses is to nutate and dephase

transverse magnetization of bulk water across a narrow frequency range (centered 4.7 ppm), while having minimal net effect on the magnetization outside of this frequency range. In each TR period, the CHESS module precedes data acquisition, in this case using PRESS. Suppression of water with CHESS results in minimal signal from water appearing in the spectrum.

**Figure 11:** Pulse sequence diagram of the PRESS with BASING modules. The three RF pulses with simultaneous gradient pulses comprising the PRESS sequence are identified as "x-localization", "y-localization" and "z-localization". The BASING modules, identified with as "BASING #1" and "BASING #2", each consists of two gradient pulses, one applied immediately before and the other immediately after a unique, long duration BASING RF pulse. The BASING RF pulse provides a frequency selective excitation centered on the Larmor frequency of the coupled proton. In the example of lactate, the coupled nucleus is the methine proton with Larmor frequency centered at 4.1 ppm. This nucleus is coupled to the three methyl protons of the lactate molecule, which generate the doublet centered at 1.32 ppm. The gradient pulses applied immediately before and after the pulse serve to dephase transverse magnetization from nuclei with Larmor frequencies near that of the coupled nucleus. For lactate, these gradient pulses also dephase the signal from bulk water at 4.7 ppm. The two BASING pulses provide excellent water suppression and obviate the need for the CHESS module.

**Figure 12:** Timing of the 90-180-180 degree RF pulses in the PRESS sequence, and timing of the two BASING RF pulses (identified by B.P. #1 and B.P. #2). The diagonal lines represent the phase progression of representative magnetization vectors at different locations within the final voxel, that evolve differently due to the underlying B0 magnetic field, but which are refocused

by the 180 degree pulses of the PRESS sequence. By separating the 180 degree pulses by TE/2, refocusing of the magnetization vectors to produce the echo will occur at time TE after the initial 90 degree excitation pulse. The time Δt between the 90 and 180 degree pulses does not affect the TE, and is usually chosen as short as possible. The BASING RF pulses invert the magnetization of only the nuclei that are coupled to the nuclei providing the signal, and they do not affect the refocusing of magnetization at TE. The BASING pulses reverse the precession direction of the J coupling effect. The figure illustrates the requirement that the two BASING pulses are separated by TE/2, for a sequence whose echo forms at TE. With this timing requirement, the precession due to J-coupling will be one direction (either clockwise or counterclockwise) for the TE/2 period between the two BASING pulses and the opposite direction for TE/2 period before and after these pulses. With application of the two BASING pulses, the J-coupling effect is nullified.

**Figure 13:** Brain lactate in a human volunteer studied with spectral editing on a 1.5T system. The top spectrum was generated using PRESS with BASING pulses applied to the methine peak at 4.1 ppm. The BASING pulse caused cancellation of the J-coupling effect and produced an upright doublet of the methyl protons at 1.32 ppm. The frequency range affected by the BASING pulse (bandwidth = 180 Hz) is indicated by a dotted-line outlined rectangle. The middle spectrum was generated using PRESS without BASING pulses applied to the methine peak at 4.1 ppm. J-coupling caused the lactate doublet to be inverted at 1.32 ppm. Peaks arising from uncoupled nuclei or nuclei coupled to protons outside of the frequency range of the BASING pulse are not affected by the BASING pulse. The difference spectrum shows cancellation of peaks unaffected by the BASING pulse. The inverted lactate doublet is subtracted from the upright doublet, leading to a larger doublet in the difference spectra. The inverted doublet has a

smaller peak area than the upright doublet due to the volume misregistration effect illustrated in subsequent figures.

**Figure 14:** Volume misregistration for lactate at TE 144 ms. Because of the chemical shift between the main nuclei (1.32 ppm) and the coupled nuclei (4.1 ppm), their volumes are not aligned. The figure shows four regions of the spectroscopy voxel, which is the volume within which the main nuclei are affected by both 180 degree PRESS pulses. Each region has a unique combination of RF pulse influence. In the Red subvolume, both the coupled nuclei and the main nuclei are affected by the first and second 180 degree RF pulses. In this region, due to J-coupling, each pulse reverses the direction of precession of the main nuclei. In the light blue region, the coupled nuclei are not affected by the first 180 degree pulse, but are affected by the second 180 degree pulse. Consequently, the precession due to J-coupling of the main nuclei is reversed by the first pulse, but not by the second pulse. In the dark blue region, the precession due to J-coupling of the main nuclei is reversed by the second pulse, but not by the first pulse. In the teal region, neither the first nor second pulse affects the coupled nuclei, so neither pulse reverses the precession due to J-coupling of the main nuclei. At TE 144 ms, volume misregistration causes the main nuclei to have different phases due to J-coupling, and the magnetization does not refocus completely.

**Figure 15:** Reduced lactate signal resulting from volume misregistration with PRESS at TE 144 ms. The four colored boxes refer to the voxel regions shown in Figure 14. In each box, the A+ and A- labels identify the magnetization contributing to the two peaks of the lactate doublet. In the Red region at TE 144 ms, the net effect of J-coupling is to add 180 degrees to the phase of

the magnetization of both peaks of the doublet, causing it to invert. However, in the other three regions of the voxel, the influence of the coupled nuclei on the doublet is different, with the light blue region adding to the inverted doublet and the teal and dark blue regions subtracting from it. For lactate at 1.5T and 3T, the Red region predominates, thus the doublet appears inverted but is reduced in size (as seen in Figure 13).

**Figure 16:** Amelioration of signal loss from volume misregistration by use of BASING pulses. The four colored boxes refer to voxel regions shown in Figure 14. The BASING RF pulses reduce the net effect of J-coupling. In the Red region, the BASING pulses cause the J-coupling effect to be reversed for TE/2, so that the net J coupling effect over the TE interval is zero. Consequently, the doublet appears upright in the spectrum in the Red region, as in the Teal region. In the light and dark blue regions, the BASING pulses reduce the net effect of J-coupling, but do not entirely eliminate it. The size of the doublet in the spectrum will be proportional to the summation of the magnetization vectors in all four colored boxes. With the BASING pulses, the doublets will be upright and nearly as large as they would have been with no J-coupling effect.

Figure 1

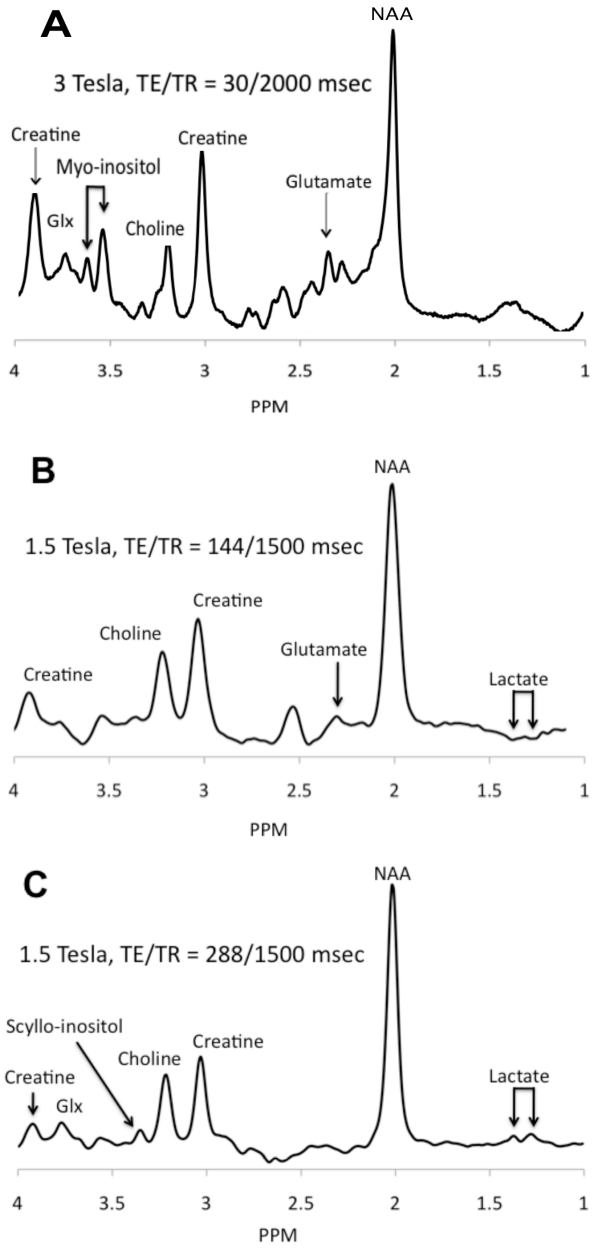
A
3 Tesla, TE/TR = 30/2000 msec
NAA
Creatine
Myo-inositol
Creatine
Glutamate
Glx
Choline
4
3.5
3
2.5
2
1.5
1
PPM
B
1.5 Tesla, TE/TR = 144/1500 msec
NAA
Creatine
Choline
Creatine
Glutamate
Lactate
4
3.5
3
2.5
2
1.5
1
PPM
C
1.5 Tesla, TE/TR = 288/1500 msec
NAA
Scyllo-inositol
Choline
Creatine
Creatine
Glx
Lactate
4
3.5
3
2.5
2
1.5
1
PPM

Figure 2

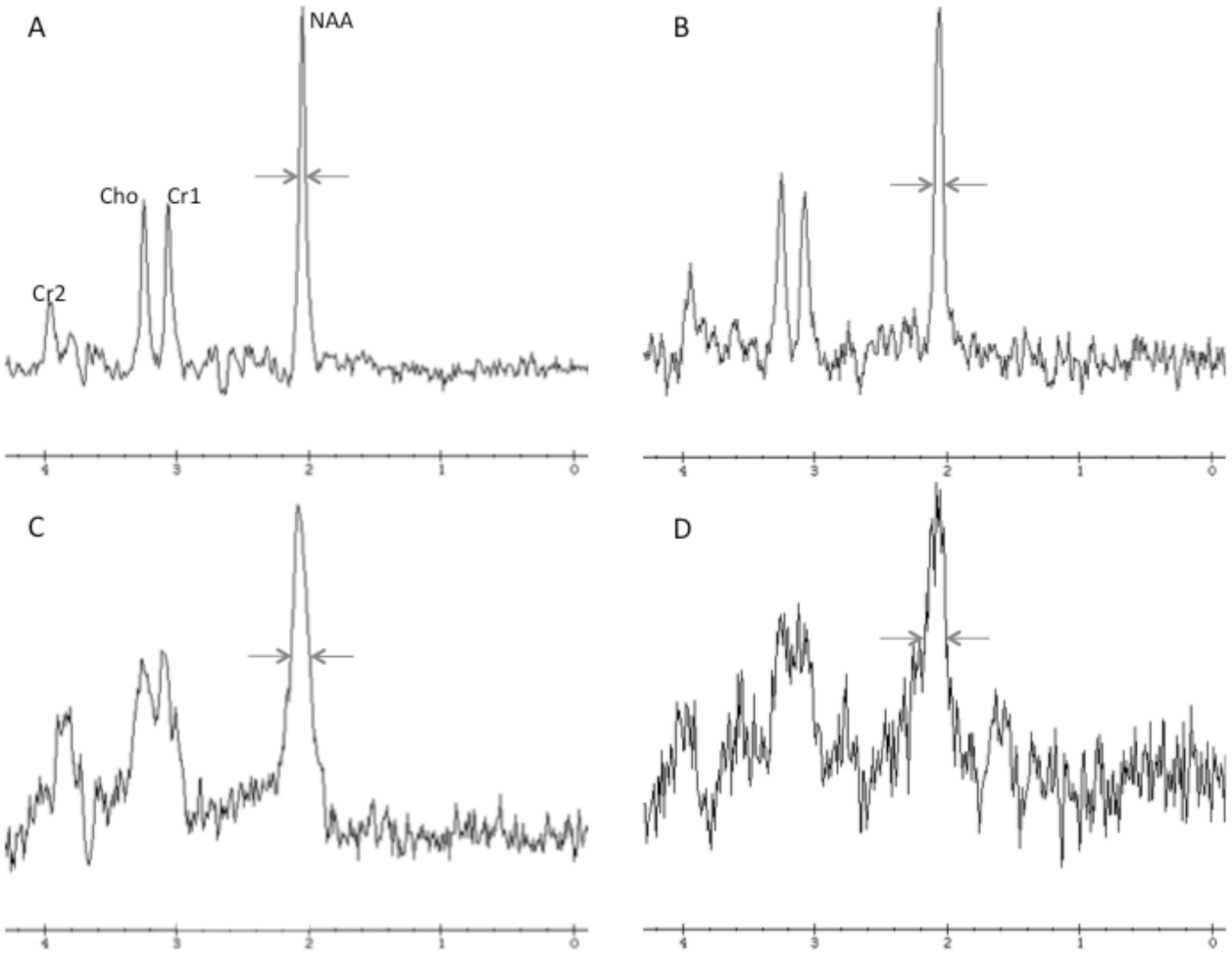

Figure 3

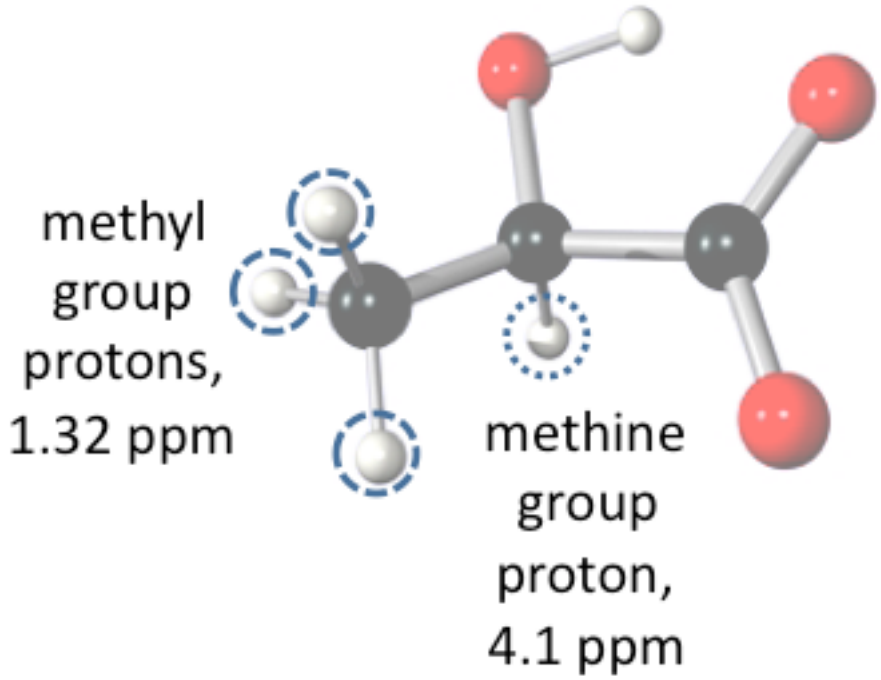

Figure 4

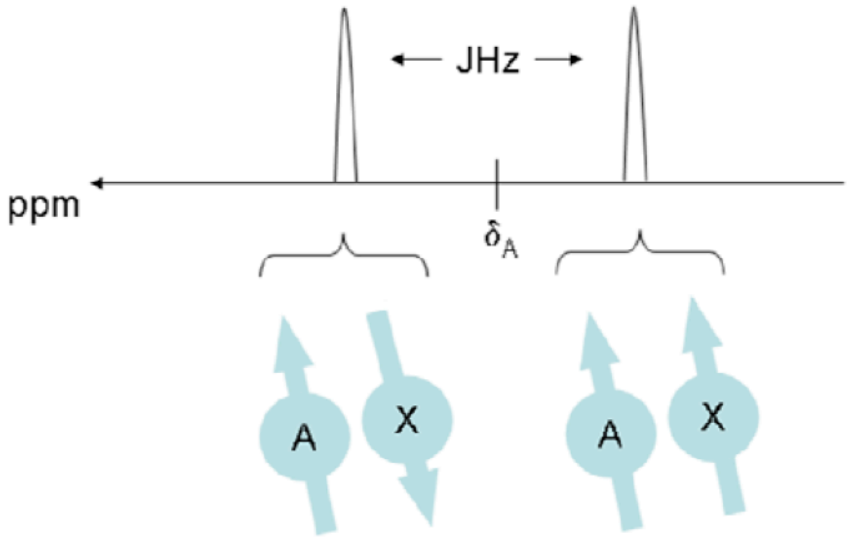

Figure 5

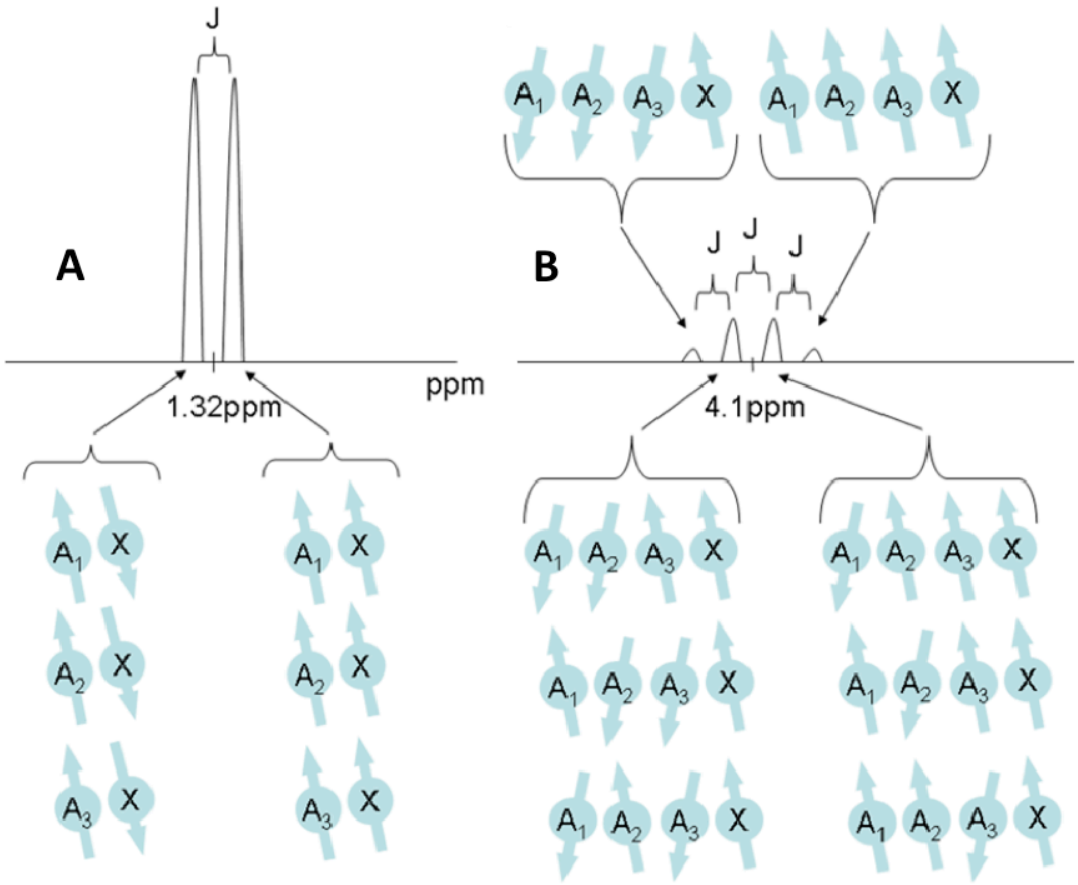

Figure 6

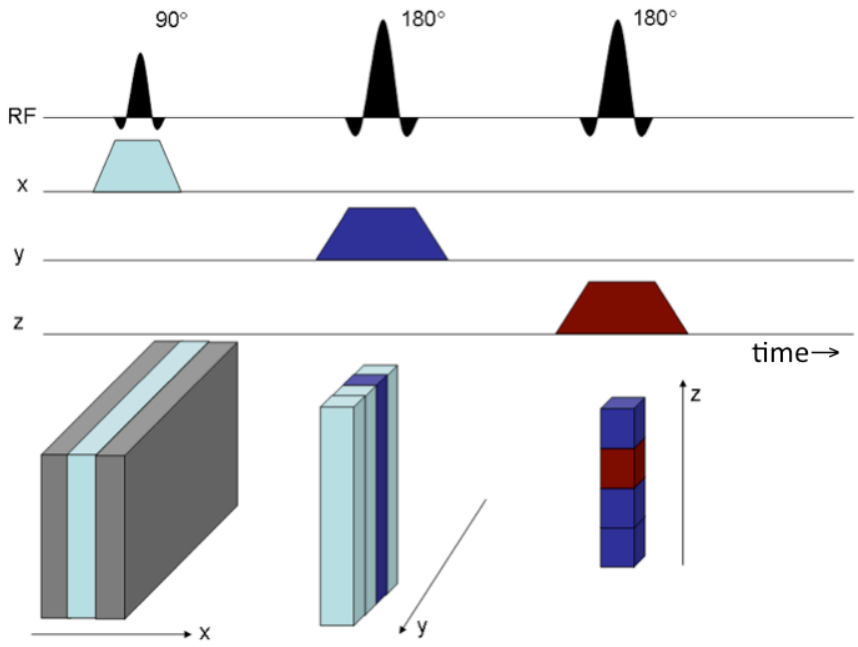

Figure 7

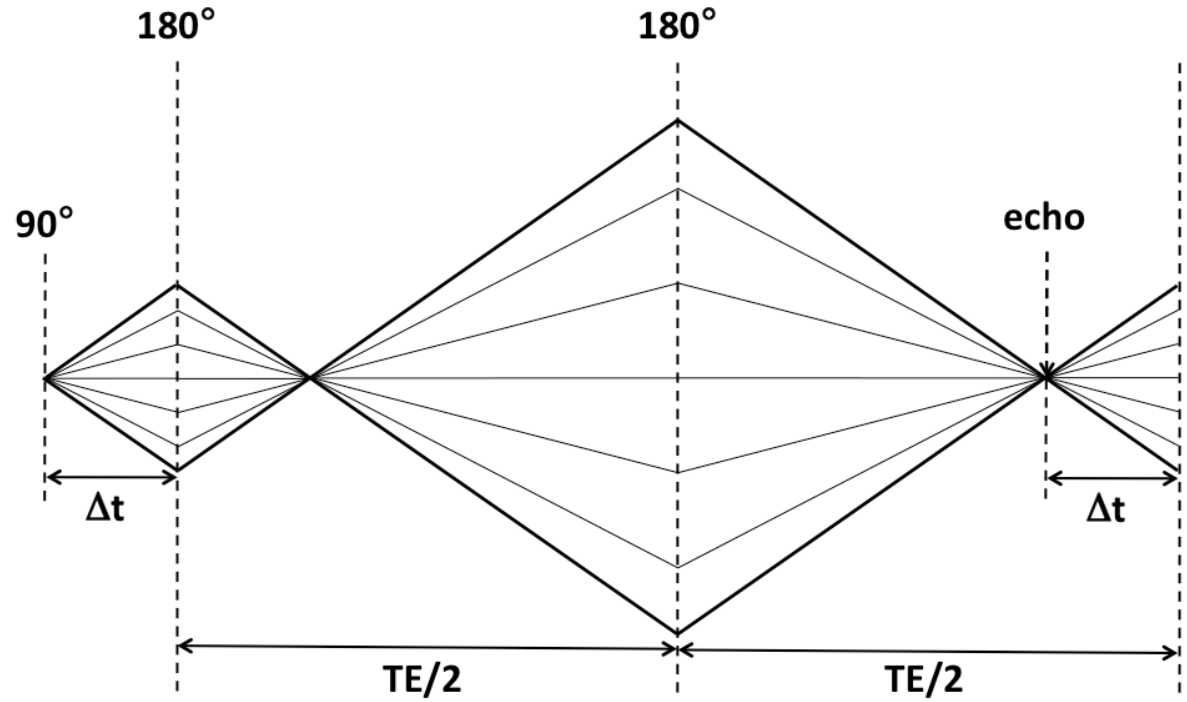

Figure 8

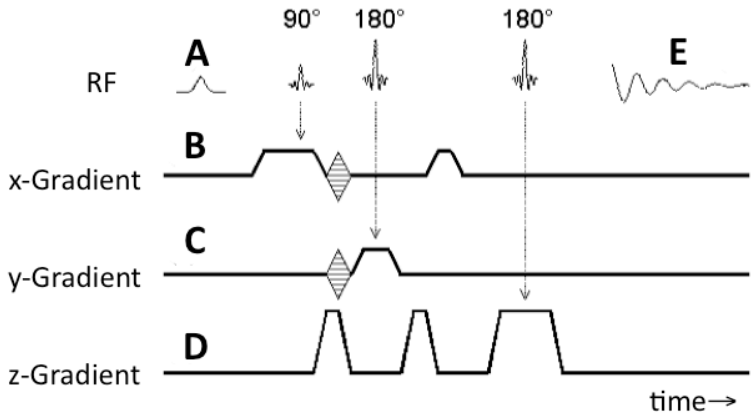

Figure 9

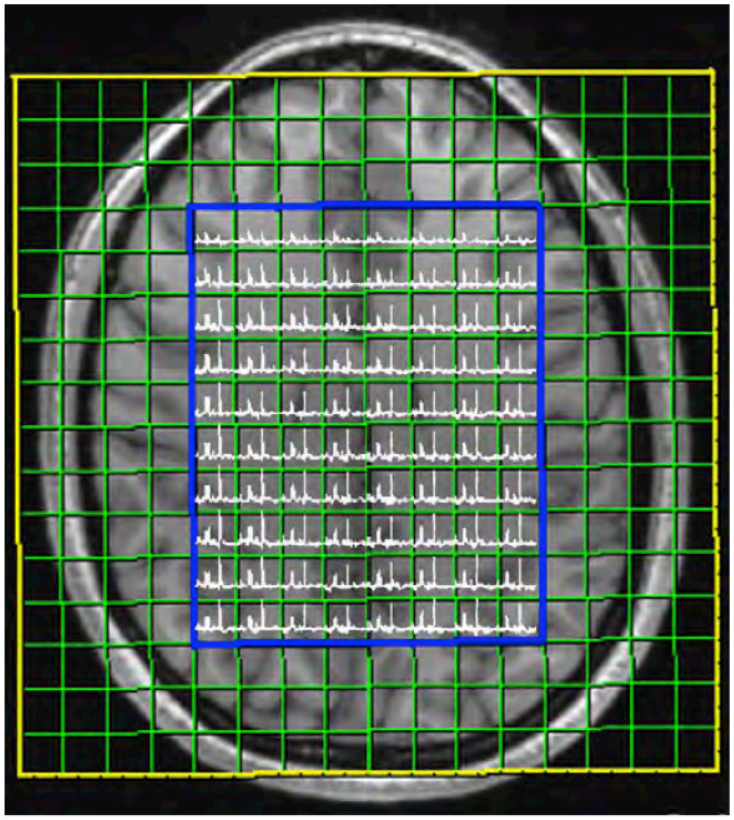

Figure 10

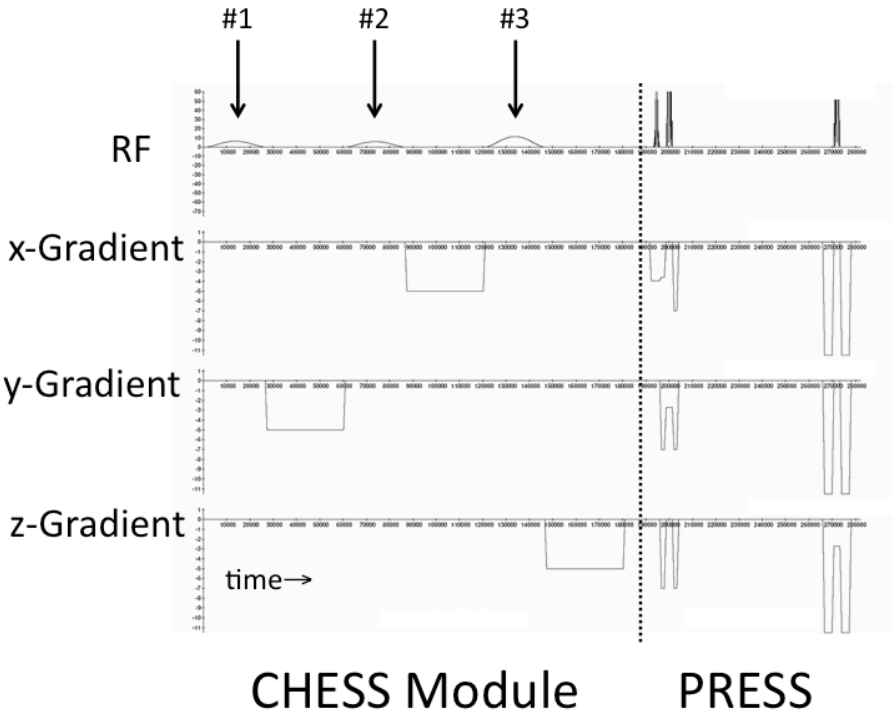
#1
#2
#3
RF
x-Gradient
y-Gradient
z-Gradient
time→
CHESS Module
PRESS

Figure 11

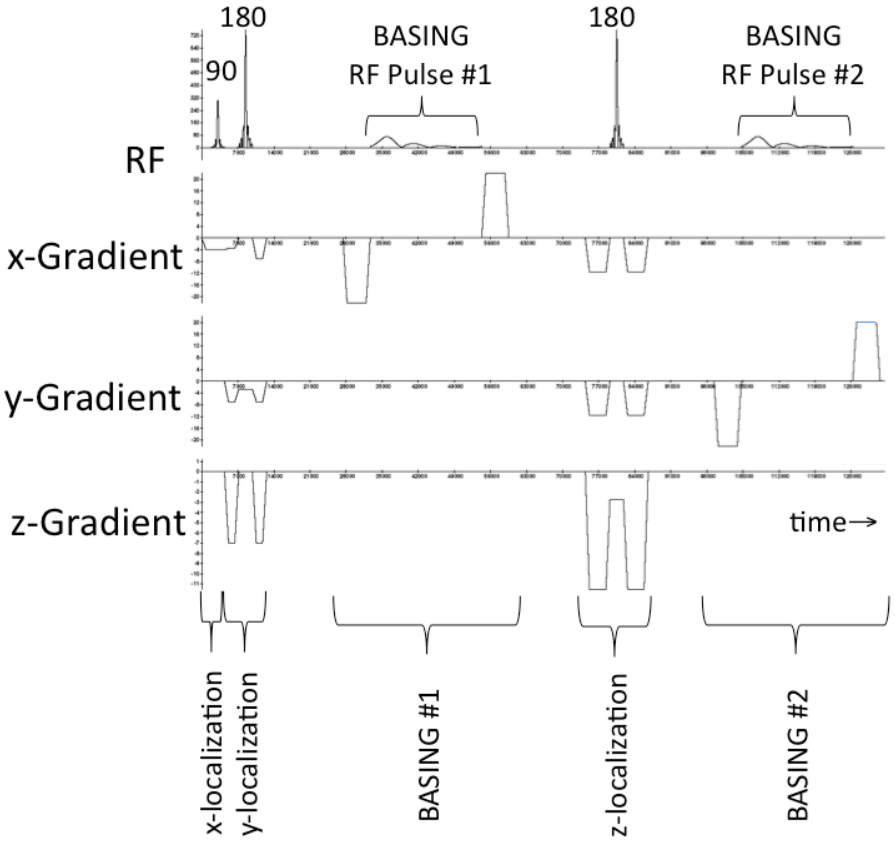
180
90
BASING
RF Pulse #1
180
BASING
RF Pulse #2
RF
x-Gradient
y-Gradient
z-Gradient
time→
x-localization
y-localization
BASING #1
z-localization
BASING #2

Figure 12

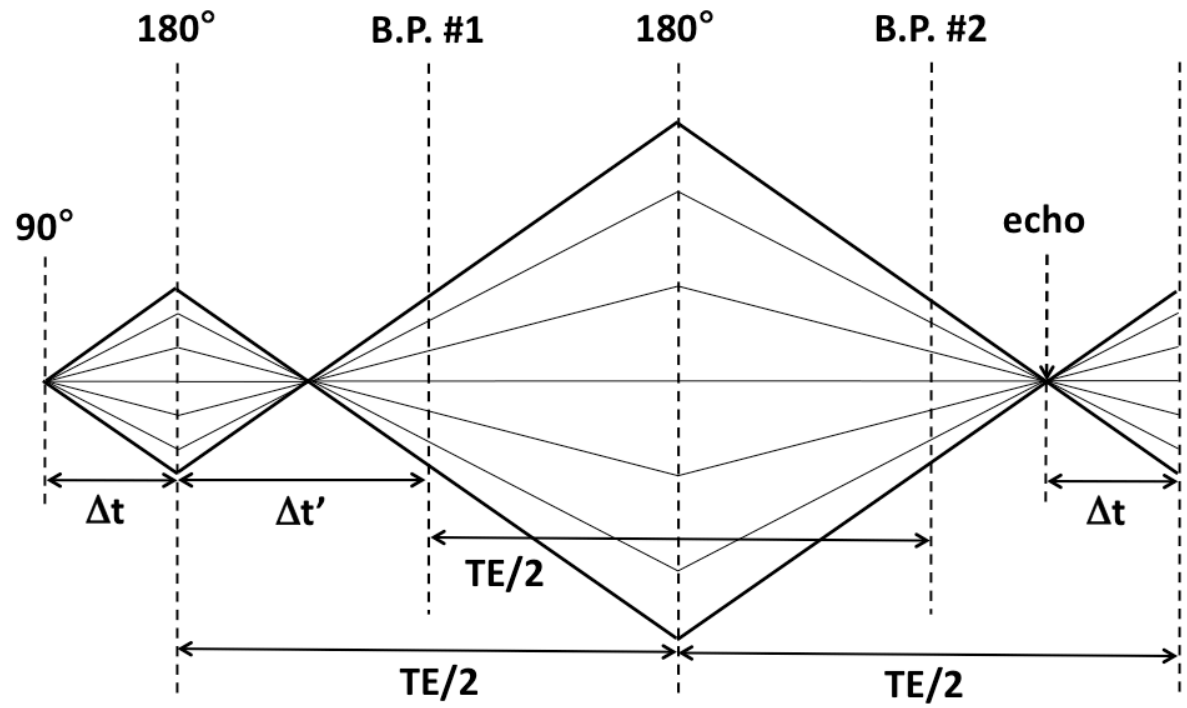

Figure 13

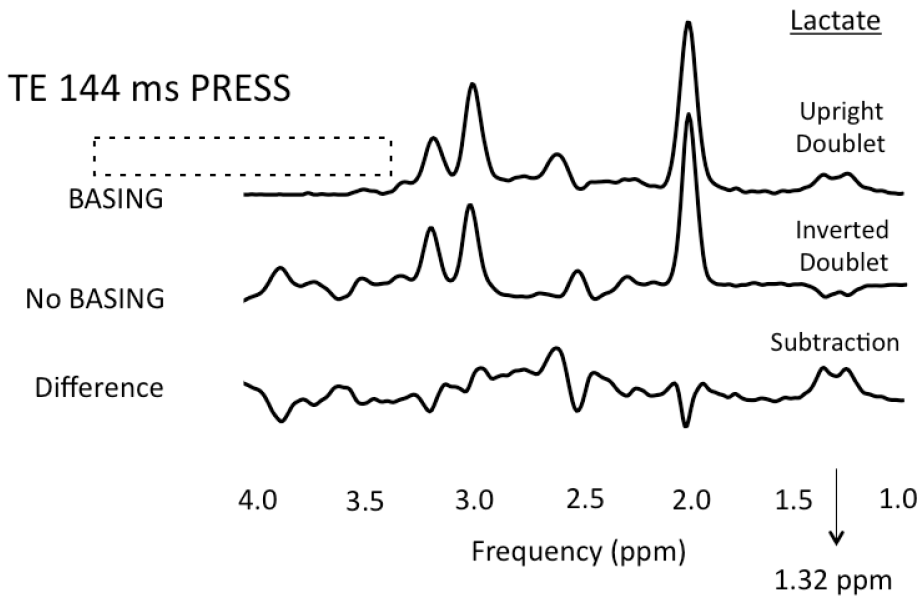
Lactate
TE 144 ms PRESS
Upright
Doublet
BASING
Inverted
Doublet
No BASING
Subtraction
Difference
4.0
3.5
3.0
2.5
2.0
1.5
1.0
Frequency (ppm)
1.32 ppm

Figure 14

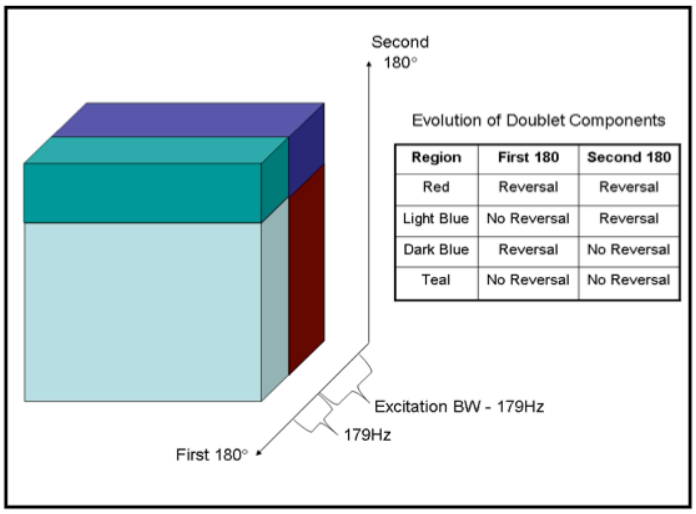
Second
180°
Evolution of Doublet Components
Region | First 180 | Second 180
Red | Reversal | Reversal
Light Blue | No Reversal | Reversal
Dark Blue | Reversal | No Reversal
Teal | No Reversal | No Reversal
Excitation BW - 179Hz
179Hz
First 180°

Figure 15

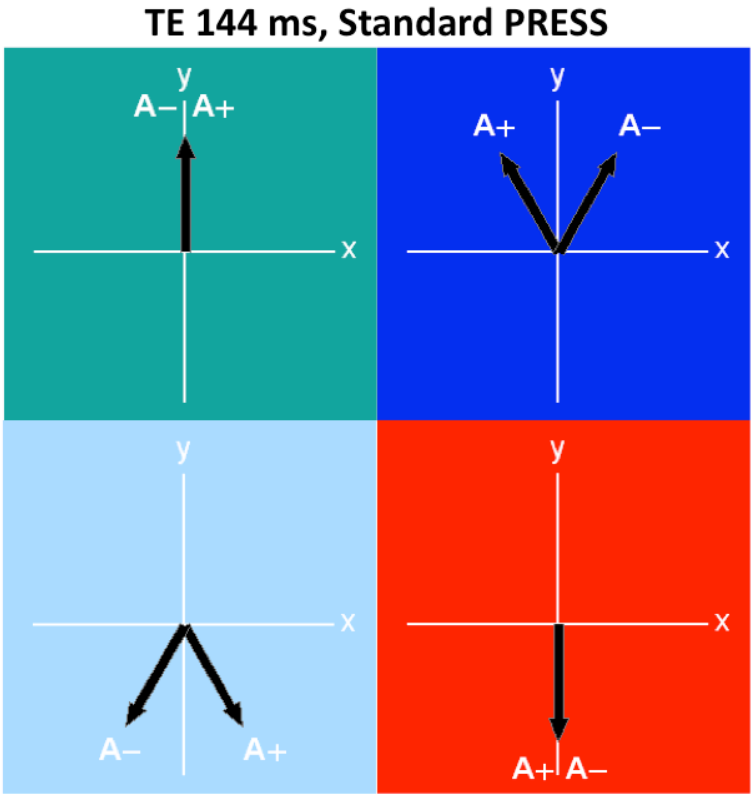

Figure 16